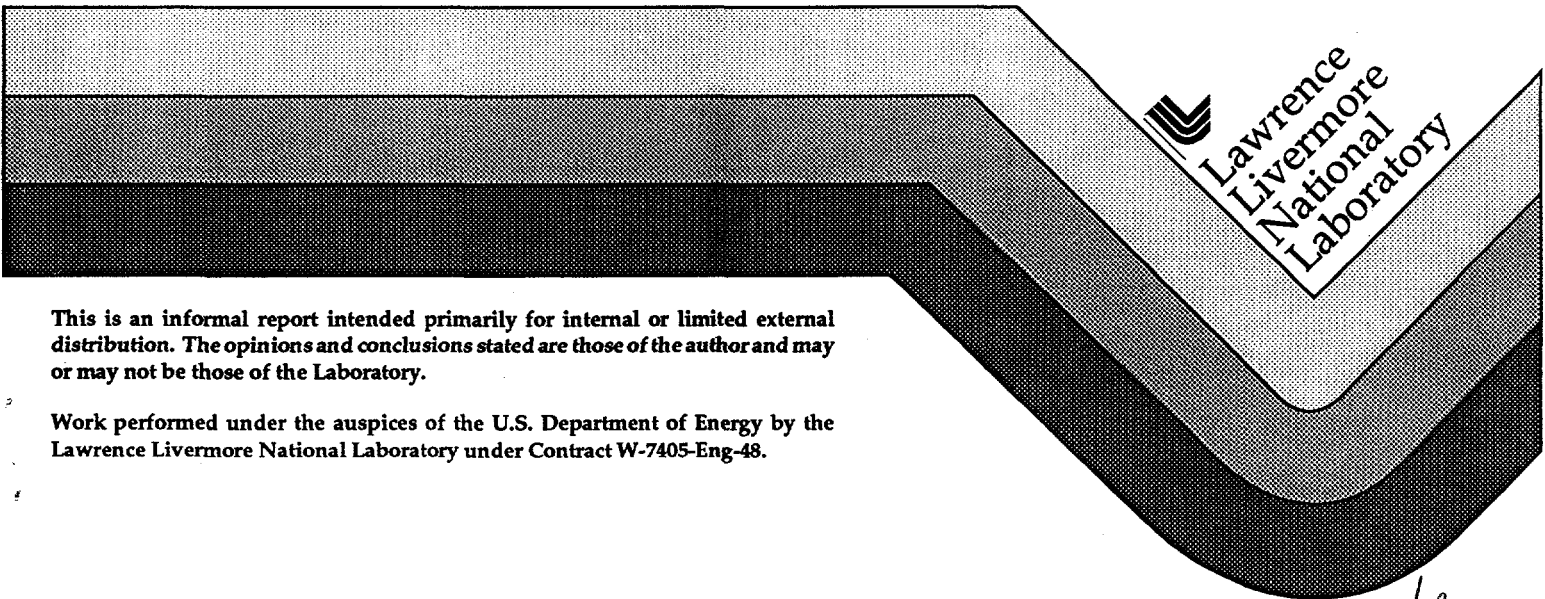


Laser Fusion Monthly - August 1980

H. G. Ahlstrom

**RECEIVED
APR 27 1998
OSTI**

August 1980



**Lawrence
Livermore
National
Laboratory**

This is an informal report intended primarily for internal or limited external distribution. The opinions and conclusions stated are those of the author and may or may not be those of the Laboratory.

Work performed under the auspices of the U.S. Department of Energy by the Lawrence Livermore National Laboratory under Contract W-7405-Eng-48.

dg

DISTRIBUTION OF THIS DOCUMENT IS UNLIMITED

MASTER

DISCLAIMER

This document was prepared as an account of work sponsored by an agency of the United States Government. Neither the United States Government nor the University of California nor any of their employees, makes any warranty, express or implied, or assumes any legal liability or responsibility for the accuracy, completeness, or usefulness of any information, apparatus, product, or process disclosed, or represents that its use would not infringe privately owned rights. Reference herein to any specific commercial product, process, or service by trade name, trademark, manufacturer, or otherwise, does not necessarily constitute or imply its endorsement, recommendation, or favoring by the United States Government or the University of California. The views and opinions of authors expressed herein do not necessarily state or reflect those of the United States Government or the University of California, and shall not be used for advertising or product endorsement purposes.

This report has been reproduced
directly from the best available copy.

Available to DOE and DOE contractors from the
Office of Scientific and Technical Information
P.O. Box 62, Oak Ridge, TN 37831
Prices available from (423) 576-8401

Available to the public from the
National Technical Information Service
U.S. Department of Commerce
5285 Port Royal Rd.,
Springfield, VA 22161

DISCLAIMER

Portions of this document may be illegible electronic image products. Images are produced from the best available original document.

KEK

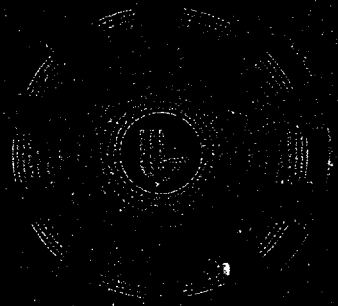
MM 80-8

93/437

August 1980

August 1980

ASSER
SON
MONTHLY



21267

This Document Consists of 67 pages

No. 23 of 74 Copies, Series A

Derivative Classifier:

Harlow G. Ahlstrom
Harlow G. Ahlstrom

MM 80 8 23A

02 MAR 89 09:19 PM UC KIDDER RAY E

LASER FUSION MONTHLY
Editor: H. G. Ahlstrom
LLNL (415) 422-5391

CONTENTS/August 1980

Classification (Declassification/Review Date) Changed to:

UNCLASSIFIED

(Insert appropriate classification level or indicate if unclassified)

by authority of R2D2-44-80-8 7/16/87 (date)

by *[Signature]* (Authority for change in classification, e.g., the memorandum number.) (date)

verified by *[Signature]* (Signature of person making the change) (date)

[Signature] (Signature of person verifying this is the correct document or model) (date)

EDITORS NOTE. 2

FACILITIES REPORT

 Shiva 3

 Argus 3

NOVA PROJECT

 Laser System 4

DATA MANAGEMENT AND ANALYSIS GROUP

 Fusion Experiments Analysis Facility . .18

DIAGNOSTIC DEVELOPMENT GROUP

 Optical/x-ray Streak Camera23

LASER FUSION DIAGNOSTIC GROUP

 Shiva Dante System Temporal Response . .29

FUSION EXPERIMENTS AND ANALYSIS

$2\omega_0$ Experiments.37

ENERGY APPLICATIONS R&D

 Planning for an Eng. Test Facility . . .59

LLNL PUBLICATIONS65

DISTRIBUTION66

Editors Note

We thank Bill Krupke, Judith Johnson, and Bonnie Knabe for their fine efforts over the last year in the production of the Laser Fusion Monthly through the June issue. Irene Freiberg, the Fusion Experiments Program Administrative Assistant, and I began our one-year assignment with the July issue. We have hired a new secretary, Beverly McCollough, who will begin in October. Our present plan is that the Monthly will retain substantially the same format, except that we are including more progress contributions from the line groups. In addition, we will have regular reports on the Halite Program. A general discussion of this joint LLNL-LANSL program was given in the July issue, and additional articles are scheduled for the September and October issues.

In August we completed the Argus experiments at $0.532 \mu\text{m}$. As predicted by the wavelength-scaling analyses, we observed increased absorption (80% at 10^{14} W/cm^2) and increased x-ray conversion efficiency (50% of the absorbed energy, also at 10^{14} W/cm^2), and noted that the scaling of the suprathermals for hohlraums follows the predicted λ_L^2 behavior. These results continue to confirm the desirability of target irradiations at $\lambda_L = 0.25$ to $0.5 \mu\text{m}$.

Facilities Report

Shiva

During August, Shiva fired 15 system shots. These shots completed the x-ray backlighter series and the density measurements using Apollo targets. The rest of the month was devoted to system maintenance.

Argus

In August, the series of 2ω target experiments was completed. Conversion of Argus to do 3ω target experiments will start on Sept. 2, and it is anticipated that 3ω target shots will commence in the second half of the same month.

Nova Project

LASER SYSTEM

The mechanical-systems design effort continued in August, and designs have been prepared for rod amplifiers, turning-mirror mounts, clean-room modifications and equipment, spatial filters, and Faraday rotators. Nova requires 15-cm and 31.5-cm Faraday rotators in addition to the rotators currently being used in Shiva. Final isolation at the 46-cm beam diameter will be accomplished with a plasma shutter located at the pinhole of the final spatial filter.

Mechanical assembly of the 46-cm disk-amplifier prototype is proceeding. All components have been received, including special complex shapes made by the electroforming process. We are pleased that we have located several suppliers who can satisfactorily fabricate the electroformed components on a production basis for the Nova chains. Functional testing of the 46-cm amplifier prototype will start this fall after delivery of the fluorophosphate laser-glass split disks. These disks will be delivered as part of the fluorophosphate development contracts we have with Hoya and Schott.

Since selecting the Nova Phase I illumination configuration (100° open cone with $f/3$ to $f/4$ lenses), we have completed the mechanical design layouts for the target bay and the optical switchyard spaceframes. These layouts include the alternative 70° geometry and provisions for Nova Phase II. Based on these layouts, we are now proceeding with detail design of the spaceframes. In addition, the spaceframes for the laser bay and the master oscillator room have been analyzed, the layouts have been completed, and the designs are being detailed.

The target-system design efforts have been focused on specifying and detailing the 2.3-m-radius aluminum target vessel. Detail design for the vacuum and other target-systems support functions is also under way.

Nova Project

Prebid visits have been made to several potential aluminum-vessel fabricators. A final design review, planned for September, will be held to authorize release of the procurement package for bid. Selection of the slower f/3 to f/4 lenses has permitted us to locate the lenses outside the vacuum target chamber; this reduces the complexity of the lens positioner and improves maintainability.

A satisfactory final design review was held for the MVA power supplies at Aydin Corp. on August 4th. Aydin is now authorized to fabricate the first production unit, which is to be delivered in November 1980. The remaining six units will be approved for fabrication after successful evaluation of the first power supply.

Evaluation of power-conditioning components continued with assembly of the plasma-shutter prototype, the ordering of additional high-density capacitors and evaluation quantities of quartz flashlamp tubes, and testing of a new type of dump resistor for the capacitor bank. The plasma shutter, the design for which was reviewed in July, will first be installed in Bldg. 611, where it will undergo functional tests in a high-electrical-noise environment. The unit will then be installed in the final spatial filter on one Shiva arm, where it will be tested to verify its ability to block full-power reflected pulses from an imploding Shiva fusion target.

We are ordering 50 quartz flashlamp tubes from Toshiba, in Japan, for evaluation based on a revised quartz-flashlamp specification. This is part of our effort to develop a second source for quartz tubing for flashlamps. Currently, Hereaus, in Germany, is our only source.

The optical components group is continuing to evaluate fluorophosphate laser-glass samples from Hoya and Schott. Hoya's latest 40-litre melt samples show some improvement from previous melts but still contain too many microscopic damage sites to be considered reliable laser

Nova Project

glass. As reported in July, phosphate laser glass is being evaluated as a backup for the 31.5-cm and 46-cm disk amplifiers. We damage tested an existing piece of Hoya LHG-8 phosphate glass and found damage beginning to occur at 29 J/cm^2 , with very few damage sites observed. This result exceeds the Nova damage-level specification of 27 J/cm^2 .

The decision date for proceeding with either fluorophosphate or phosphate glass is the end of October 1980. The final decision will be based on the relative abilities of Hoya and Schott to solve the damage problem and on comparative costs of the two glasses. The costs per unit volume of phosphate glass appear to be half those of fluorophosphate glass, with only minimal performance penalty at short pulse widths (less than 1 ns) and with comparable performance at pulse widths ranging from 1 to 5 ns.

We found a variance in the strain birefringence test results on our FR-5 Faraday rotator glass. The Hoya results differed from ours. After consultation with Hoya we agreed that they had incorrectly measured the birefringence; consequently, we have instructed them on the proper measurement procedure and have returned the glass to them. Hoya will reanneal the glass to correct the problem and retest it with the revised procedure.

Designs for the primary laser-system sensors for the alignment, diagnostics, and control systems are continuing with final assembly of the LLNL input sensor and detail design of the Aerojet Nova output sensor. The prototype input sensor is in final assembly in our Electro-Optics lab, and optical-bench performance tests are planned for September. Earlier tests on a filter-wheel/charged-coupled device (CCD) camera mount (see Fig. 1) indicated that, when the wheel stops, excessive vibrations are set up that confuse the encoder. This problem is being corrected by changing the gearing of the wheel to make it more rigid.

Nova Project

Additional CCD camera tests have confirmed the sensitivity and resolution characteristics of the encoder. These tests, which were performed on the third unit assembled, provided results consistent with those obtained on the first two units. The latest unit was also operated at 2ω and with pulsed signals, whereas earlier units were only tested at 1ω and with CW signals.

The Aerojet Nova output-sensor design is in final design. It is being optimized for use at three laser wavelengths. All of the features for every sensor function have now been designed. Aerojet is proceeding with the detailed mechanical layout.

NOVA CENTRAL CONTROLS

Introduction

In April 1980, at a Nova design review, we presented the state-of-the-art central-control-system architecture, selected from several alternatives, that we considered to be the most cost-effective improvement over the Shiva control system. The selected architecture, shown in Fig. 2, was established as our baseline for design.

Several major development efforts were identified and reviewed as part of the plan to provide the most reasonable and cost-effective approach which emphasizes integration, centralization, commonality, reliability, and flexibility, to meet present and future performance criteria for Nova controls.

We received approval at the review to proceed with development of the major items described and to design the Nova control system with its computers so that it can always be operated in an unclassified manner. As with Shiva and Argus operations, the Nova control room and target area

Nova Project

will be secured during classified operations. Certain target data will be shipped to a secured computer (VAX) in Bldg. 381, using a one-way data link, and portions of the television system will be interlocked to prevent access to classified images by either computer or unauthorized personnel. Also, it was agreed that the layout of the central control room would be modified to provide a single operations center with four consoles, as shown in Fig. 3.

Major Development Efforts

Since the design review, the following major development efforts have received concentrated attention.

Operator Consoles. The central operator consoles will each contain three high-resolution, high-speed, color video displays mounted in an equipment rack. Physical dimensions of these displays will be optimized for comfortable use by one experienced operator. A touch-panel input device will be mounted on the center video display. The console hardware and software, and, indeed, the entire control-system architecture, will interchangeably support status inquiry and control of any control subsystem from any of the four consoles.

Image Analysis. Hardware and software packages are being developed to provide standard analysis functions, including focus measurement, focused-spot position measurement, beam position measurement, and color enhancement of measured laser-beam characteristics. A high-speed video digitizer and an array processor that will be interfaced to the VAX computers, together with software being developed, will be employed to provide these analysis capabilities. One major use of these packages will be within the closed-loop alignment of the laser system.

Nova Project

Praxis. A high-order computer language designed for efficient programming of control and systems applications, Praxis is being developed for use in controlling the Nova laser. This language is a comprehensive, strongly typed, block-structured language in the tradition of Pascal, with much of the power of the languages Mesa and Ada.

In January 1979, LLNL funded Bolt, Beranek and Newman to augment the design of the language and to implement a compiler for the PDP-11 series of computers. Follow-on efforts have included the VAX computer, documentation, additional language design, and a high-level input/output package. Completion of the Praxis effort is scheduled for December 1980 with the delivery of documented operational compilers written in the language itself.

Novalink/Novanet. The Novalink/Novanet system is a high-speed (10 Mbit) fiber-optic technique for computer-to-computer and computer-to-device communications. Low overhead on the computers is assured by implementing much of the message protocol and data transfer operations within the hardware of the interface units instead of in computer-resident software. This communication method will be employed throughout the Nova alignment and diagnostics distributed-control systems.

Input/Output Controllers (IOC). These IOC units use multipoint memory with connections to each VAX computer and to one of the major control subsystems: power conditioning, alignment, laser diagnostics, and target diagnostics. The units optimize and efficiently handle the details of interactions, including control-system commands originating from the VAX, operational interlocks, event logging, notification of status changes and command completions, reservation of devices, and waiting for events. The units also provide a uniform control-system view of the system state for all computers and programs in the system.

Nova Project

Other Development Efforts. Several other major areas of development were briefly described in the design review, including control and display data-base design and use, Novanet software support, the event logger, subsystem operational interlocking, and the shot scheduler.

Accomplishments

Since the design review, substantial progress has been made on the major developments in an order planned to make most effective use of our resources:

- o A prototype operator's console, now standing in our Control System Development Lab, has demonstrated the graphics-analysis software package that drives the color video displays.
- o Praxis, even in its present, unfinished, state, has now replaced Fortran as our control-system implementation language.
- o Particularly noteworthy are both the prototype software being developed for power-conditioning control and the software internal to the stepping-motor controllers that will be used throughout the alignment system.
- o Novanet hardware in small quantities now exists, and point-to-point communications between the VAX, an LSI-11, and general I/O devices has been accomplished. CCD-array camera data have been successfully transferred over Novanet links.
- o A multiport memory with special interrupt-handling features has been successfully interfaced to our VAX computer--a first for a VAX anywhere. A high-speed array processor has been interfaced to the VAX, and many of its features are operable.
- o A central-control data base has been designed, and many key portions have been programmed and tested.

Nova Project

Conclusion

We are in a strong position to begin applying the major developments in the central-control system, described above, to actual control and data-acquisition problems. In October, we plan to demonstrate the capabilities developed to date as they apply to a closed-loop laser-alignment problem that is now being set up in the Control System Development Lab.

LABORATORY BUILDING

Construction of the laboratory building has progressed to the stage where photographic coverage of the total building can no longer give a proper perspective of the actual progress. With the exception of installation of the steel siding, all of the effort is now taking place inside the building:

- o The laser-bay concrete floor and the first-floor lab-space slab above the computer room have been poured, as has the footing for a shielding door and the diagnostics loft.
- o The target-room roof forms and the laser-bay slab forms have been removed, and sandblasting of the exterior concrete has started.
- o The structural-steel floor decking has been completely installed.
- o Installation of the electrical substation has started, all duct banks are complete, and installation of conduits in the concrete floors is continuing.
- o Embedded roof drains and duct and pipe hangers are being installed.
- o Offsite shop fabrication continues on the shield doors, metal siding, and metal roofing.

Nova Project

Following recommendations of the internal audit that was conducted on the conventional facilities assurance program audit in July, LLNL Plant Engineering has assigned a dedicated onsite project team to support Nova for the remainder of the conventional construction. This team will be located in its own office trailer adjacent to that of Kaiser Engineers at the construction site. Assignment of this team will provide continuity of effort and will ensure that field or A-E design changes are properly reviewed for consistency with our design criteria. Other audit recommendations will result in an improved deficiency reporting form and review procedure.

OFFICE BUILDING

Final interior-design selections of colors, carpets, and finishes for the office building are being made. Sandblasting of the concrete towers was completed, but the work does not meet the architectural finish criteria. We have rejected the work and are meeting with DOE/SAN and the contractor to resolve the problem.

NOVA BEAM ALIGNMENT CCD IMAGER

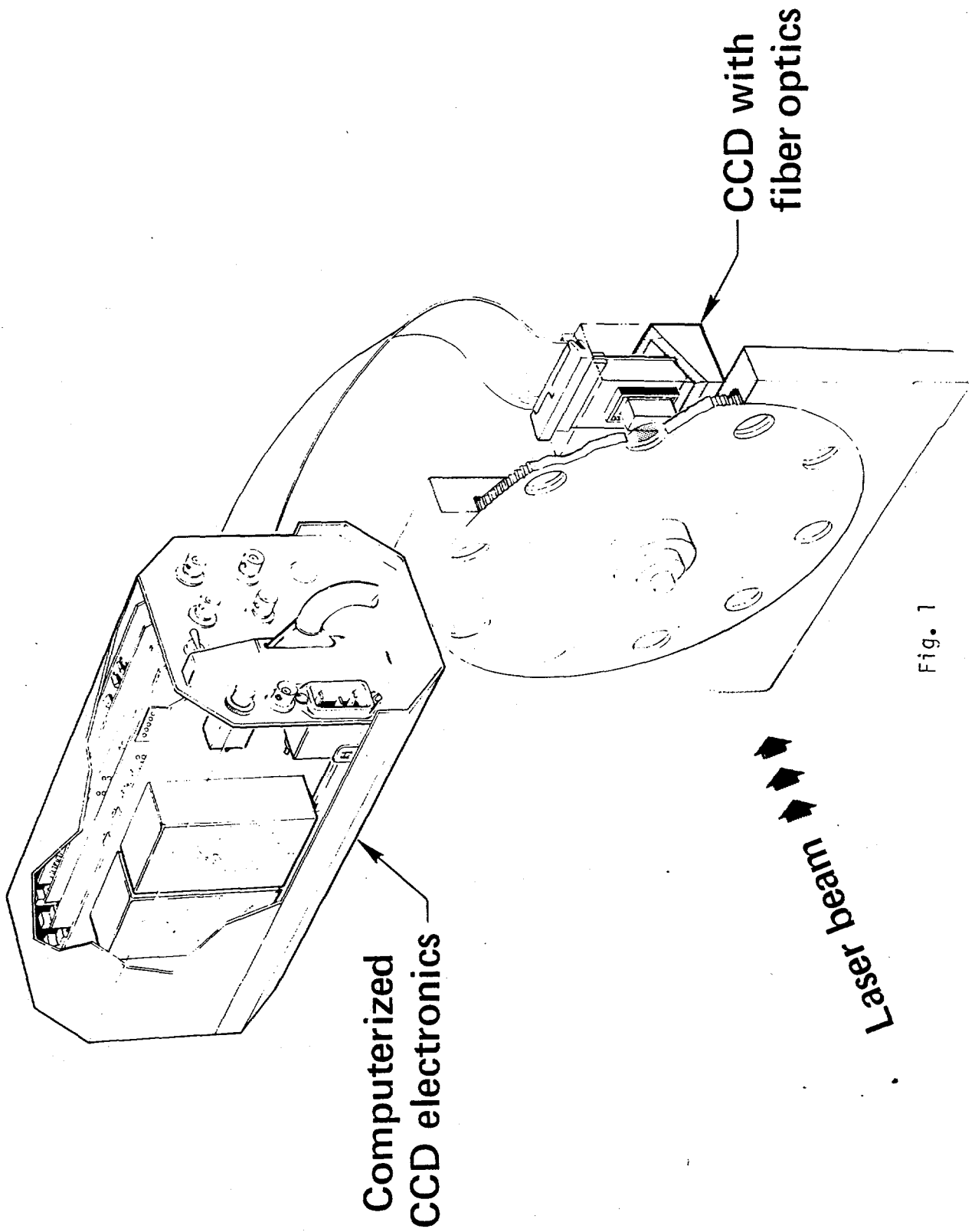
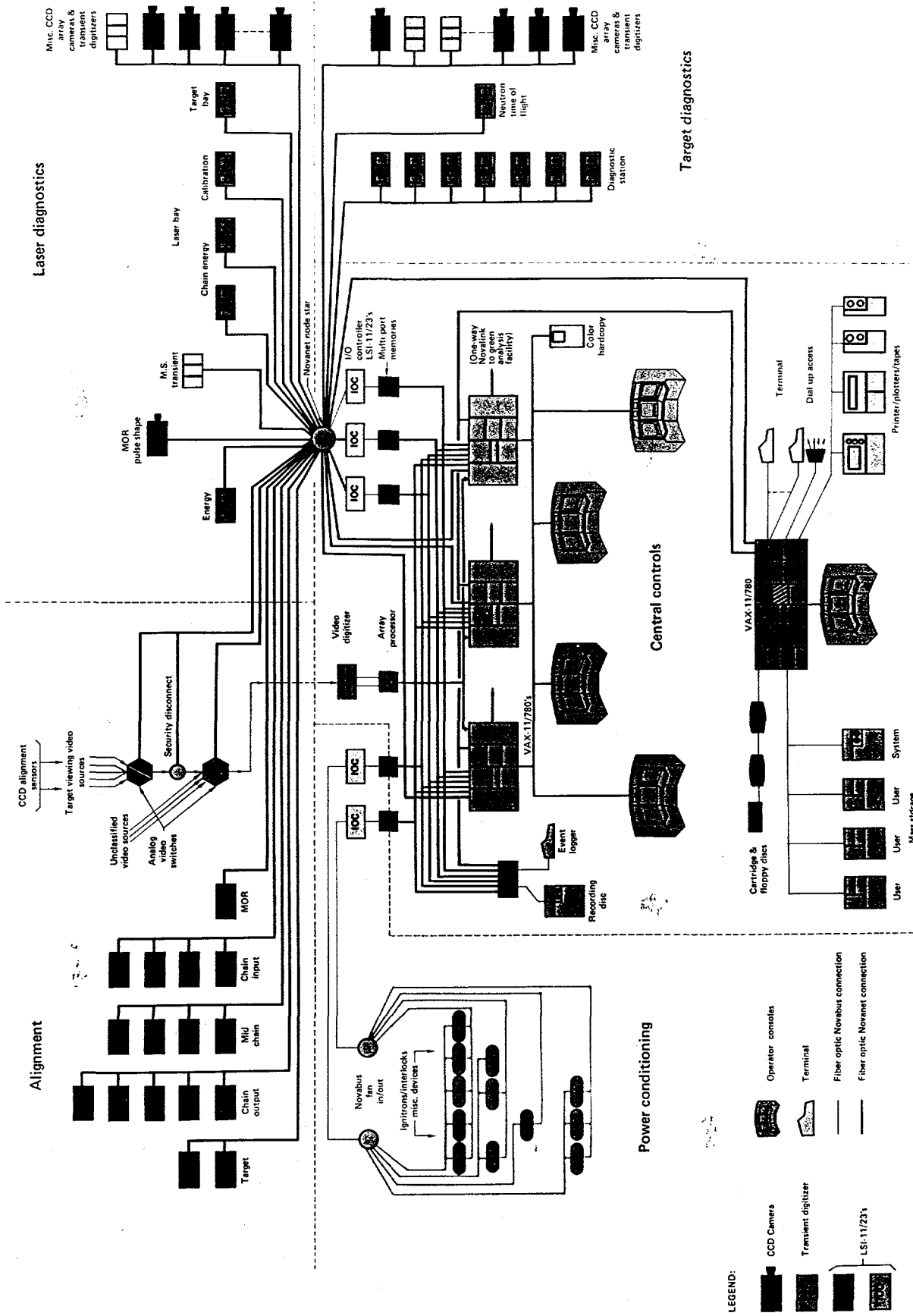


Fig. 1

*This page intentionally
left blank.*

NOVA CONTROL SYSTEM ARCHITECTURE



Red Development & Analysis

Fig. 2



NOVA CONTROL ROOM

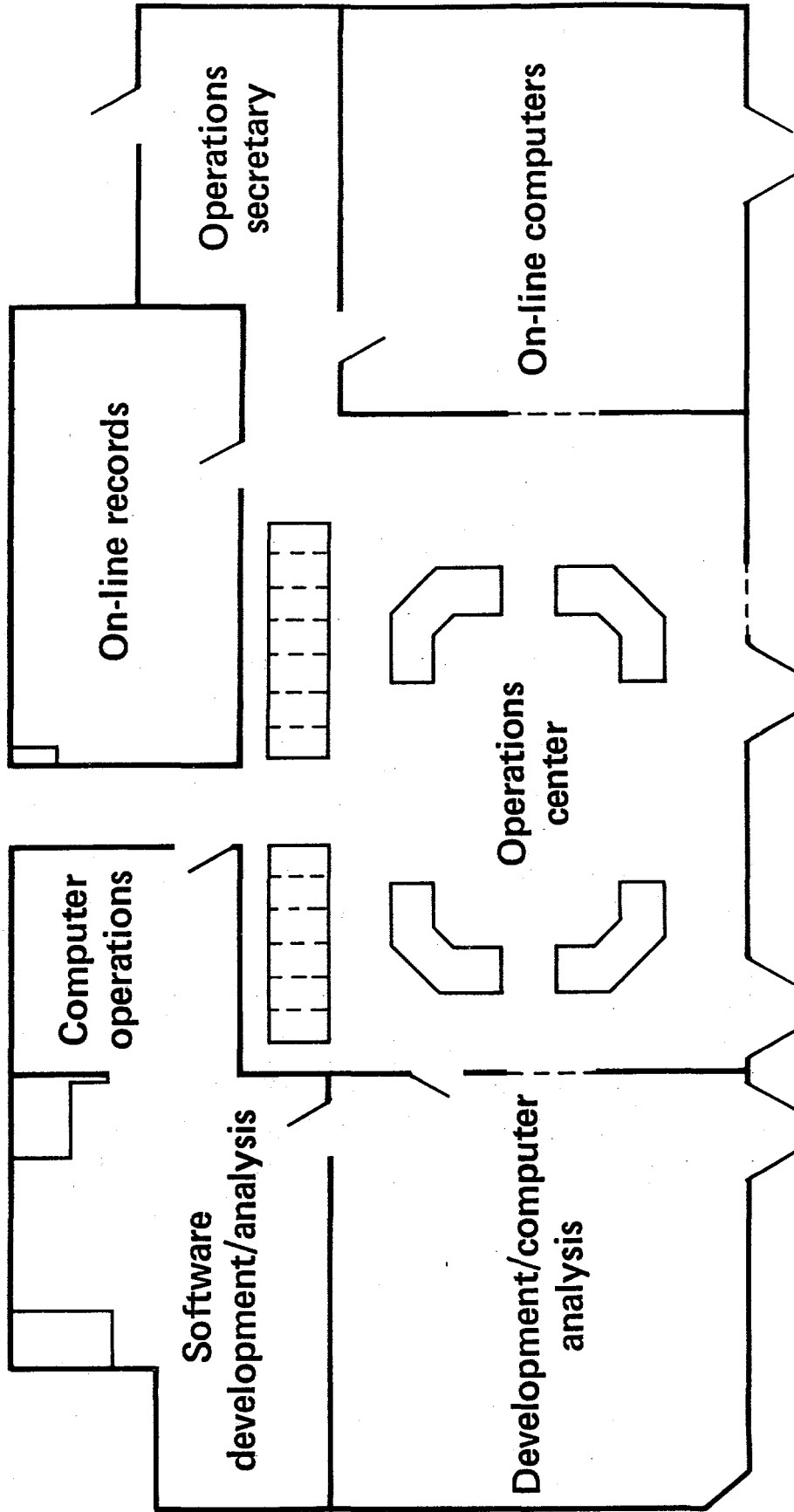


Fig. 3

Data Management and Analysis Group

FUSION EXPERIMENTS ANALYSIS FACILITY

As more diagnostics have been added to the Argus and Shiva lasers, there has been a substantial increase in the volume and complexity of the subsequent data analyses. One of our goals has been the speedy in-depth analysis of target and laser diagnostic data. The fusion-experiments analysis facility (FEAF) was designed to accommodate the data reduction and analysis needs of the Argus and Shiva facilities as well as future requirements arising from the Nova facility. As designed, FEAF will handle up to 15 simultaneous users without loss of efficiency.

After careful review of the data flow and the analysis codes, we established that the most efficient way to handle and analyze the target and laser diagnostic data was to acquire and place in one facility the necessary computational resources. It is necessary that this facility be classified and be located near the personnel responsible for data analysis. Classified and unclassified data from Argus, Shiva, and Nova will be directly transferred to FEAF via one-way fiber-optics communication links. This data-transfer mode will permit the operation of Nova as an unclassified facility except during the brief periods when classified shots take place (as is now done with Argus and Shiva).

A schematic design of FEAF is shown in Fig. 4. After a shot is made, target and laser diagnostic data will be transferred to FEAF, and the reduction and analysis will begin immediately. The main processor in FEAF will be a VAX 11/780 computer, which has sufficient computational speed and memory to handle all the data from our experiments. If very large number-crunching analyses are required, we will use a link into the LLNL Octopus computer system.

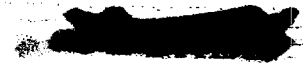
An important feature of FEAF is a digital image-processing and graphic-display capability designed to facilitate the analysis of x-ray images and streak-camera data. The image-processing hardware will consist of CRT color displays and a hard-copy color camera.

Data Management and Analysis Group

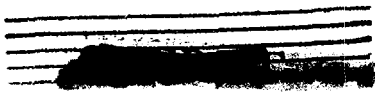
From January through March, we completed the system design and obtained DOE approval for the overall design and for major hardware purchases. In April and May, we placed purchase orders for the long-lead-time items.

Because of inadequate space in Bldg. 381, a building addition especially designed to house FEAF is now under review. Until the new building is operational, FEAF will be housed in trailer 3725. Remodeling of this temporary facility, which will include additional power, air conditioning, and fire protection, will be completed in September.

While a few pieces of hardware have already arrived, we are experiencing some delay in deliveries by some manufacturers. Nevertheless, we anticipate that partial operations will start as scheduled in the first week of October. FEAF is expected to be fully operational, except for the one-way data link to the facilities, by the end of December. The data link will be installed when FEAF is moved to its permanent location.



*This page intentionally
left blank.*



FUSION EXPERIMENTS DATA ANALYSIS FACILITY

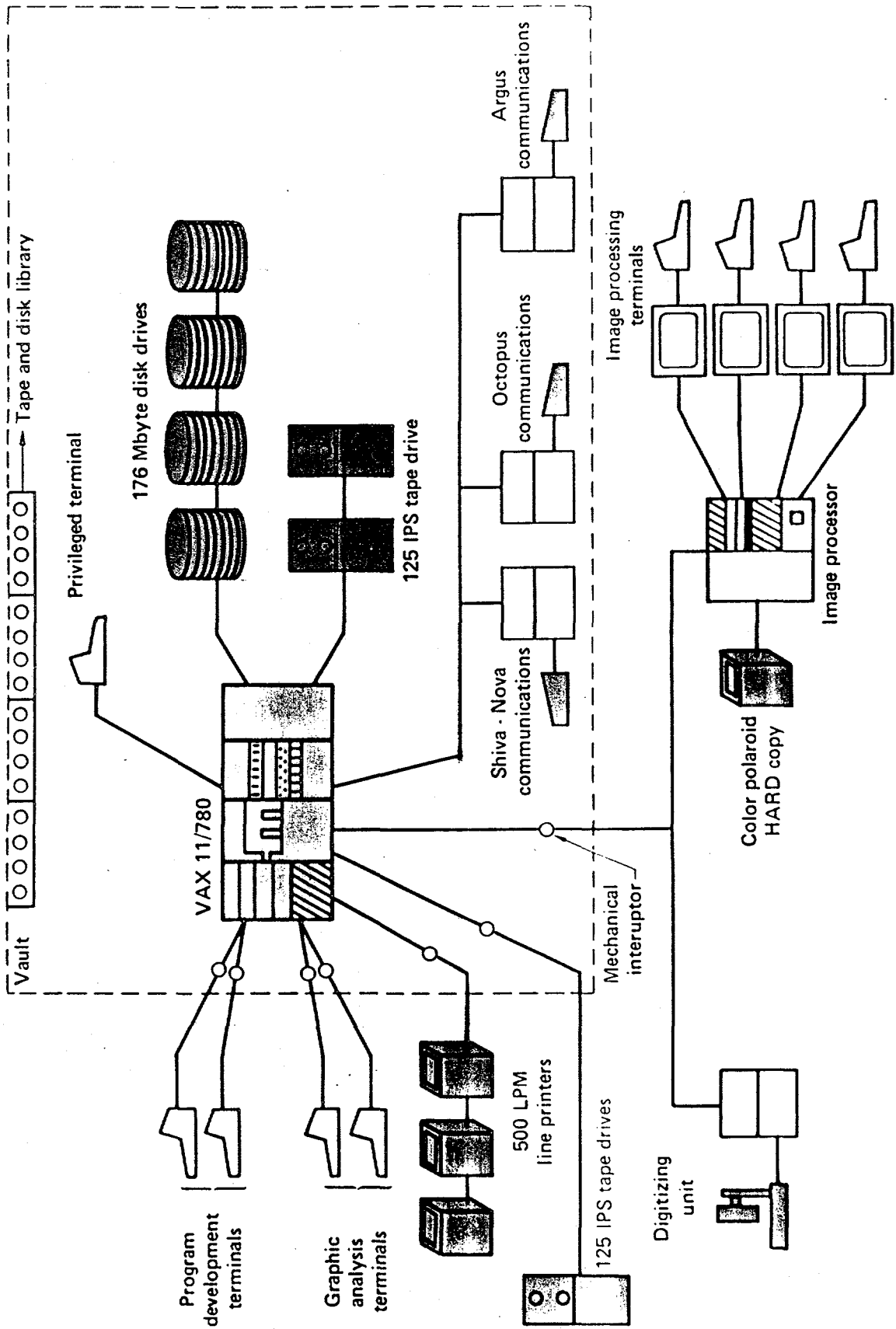
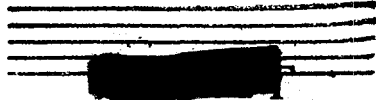


Fig. 4

60-00-0280-0583



*This page intentionally
left blank.*



Diagnostic Development Group

OPTICAL/X-RAY STREAK CAMERA

The generation of suprathemal electrons is a significant issue within the laser program. If we are to better understand the processes involved, and to better model their effects on target implosions, it is important that we know the temporal evolution of suprathemals with respect to the driving pulse. To obtain such data with good temporal resolution (10 ps) and dynamic range (10^3) on a single instrument, we have recently used one of our usual S-1 optical streak cameras to simultaneously record both unabsorbed 1.06- μm laser light and suprathemal (≈ 30 keV) x rays generated at the target.

Although designed for visible and near-infrared photons, the S-1 photocathode, which contains silver and cesium, is moderately efficient for the detection of x rays. The major limitation in these early experiments is the 2.8-mm glass window; this window absorbs x rays below about 25 keV, thus preventing them from reaching the photocathode. To somewhat improve the sensitivity of the streak camera, we increased the camera slit width from the standard 50 μm to 500 μm for these experiments, resulting in a small degradation of temporal resolution. In fact, the contacted slit is cut through a 6-mm lead sheet to prevent x rays from penetrating the usual streak-tube entrance window and interacting directly with normally unused photocathode areas and the streak-tube output phosphor.

Typical data from one of our early experiments are shown in Fig. 5a. Time proceeds vertically as indicated by the arrow. The optical signal on the left has been transmitted through a 1.06- μm band-pass filter, which blocks other visible wavelengths, and through 0.75 in. of lead glass, which blocks x rays. The x-ray signal on the right is filtered by tin and aluminum foils, which block 1.06 μm and other visible radiation. Figure 5b

Diagnostic Development Group

shows temporal signatures of the 1.06- μm laser and 30-keV suprathreshold x-ray signals; these data were obtained by taking lineouts of the raw data shown in Fig. 5a and correcting for recording-film characteristics. Note that, in this particular experiment, the suprathreshold x rays were generated early in the envelope of scattered 1.06- μm light. The shape of the suprathreshold x-ray signal, as recorded with the camera we call OX-1, is in good agreement with that recorded with our usual x-ray streak camera (X-1), which is not sensitive to 1.06- μm light. This agreement, which was seen throughout the series, is doubly interesting because the X-1 camera is also sensitive to thermal x rays.

Having developed an ability to unambiguously record optical and x-ray signals with a single streak camera, and having obtained some significant data that affect our modeling of target performance, we are now actively pursuing three experimental improvements:

- o We are using a wider (3 mm) slit and a different streak-camera focusing procedure to increase the camera sensitivity by a factor of 12 without loss of temporal resolution.
- o We are feeding part of one 1.06- μm incident Shiva laser beam directly to the camera via a fiber-optic link. This procedure will allow us to compare the x-ray signal with both the incident and the unabsorbed laser-light envelopes.
- o We are having ITT/Fort Wayne construct a modified S-1 streak tube with a thin (8 μm) mica window that will extend our lower x-ray energy limit to about 2.5 keV. This modification will enable us to use a single instrument to unambiguously detect incident and scattered laser light and suprathreshold and near-thermal x rays.

Diagnostic Development Group

Figure Captions

- Fig. 5a. Streak camera photograph showing simultaneously detected x rays and unabsorbed 1.06- μm laser light. The optical signal is on the left and the x-ray signal is on the right. The central region where the optical and x-ray filters overlap is a background measurement of the high energy x rays that penetrate our shielding and interact in the photocathode and output phosphor.
- Fig. 5b. Temporal characteristics of the 1.06- μm laser and \approx 30-keV x-ray signals shown in Figure 5a. Curves are obtained by taking lineouts of raw data and correcting for film characteristics. Our preliminary measurements have 25 ps resolution. The absolute timing error between the two signals (caused by film alignment during the reading process) is known to be less than 50 ps.

*This page intentionally
left blank.*

SCATTERED 1.06- μm LASER LIGHT AND HIGH ENERGY ($> 30 \text{ keV}$)
 X RAYS SIMULTANEOUSLY DETECTED WITH AN LLL OPTICAL
 (S-1) STREAK CAMERA



500

Raw data

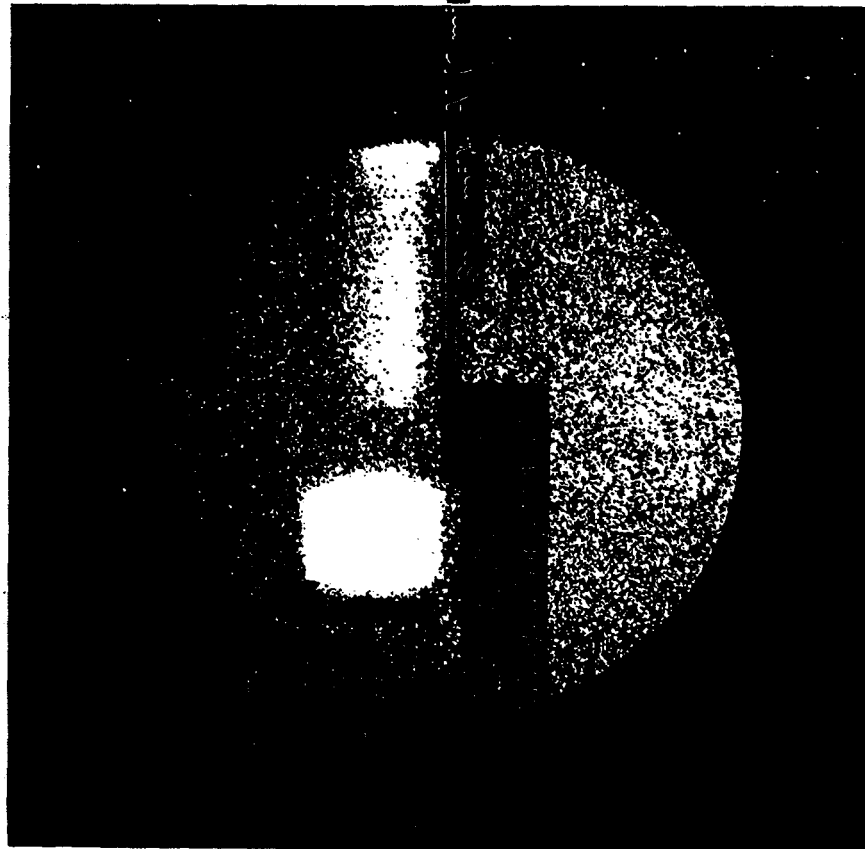
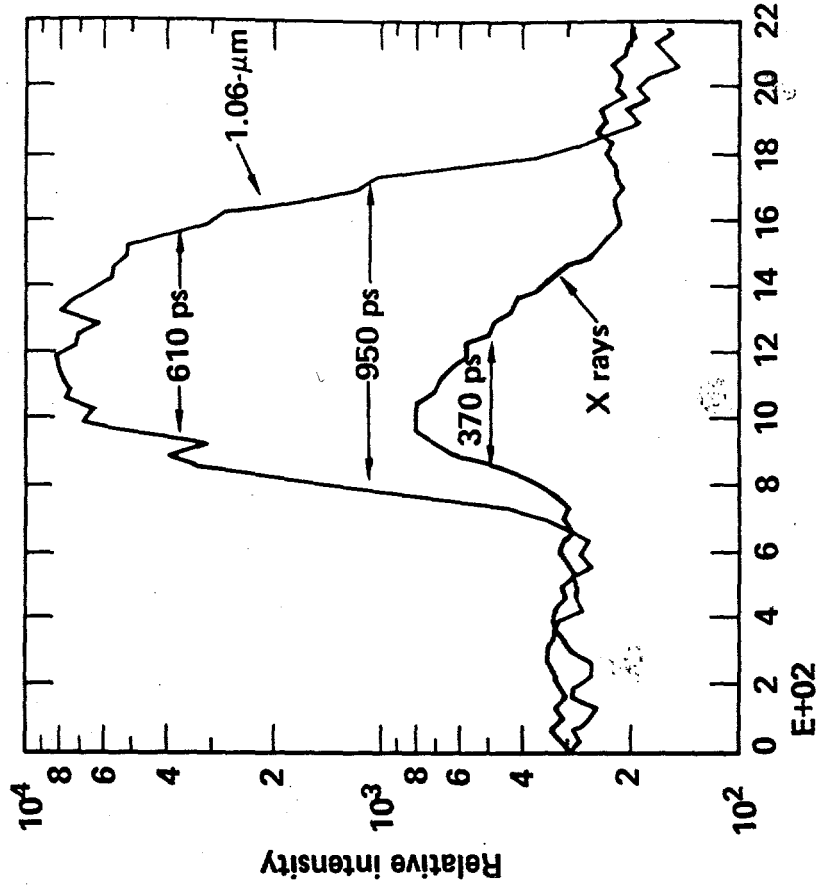


Fig. 5a



Time (psec)

Fig. 5b

[REDACTED]

1997

[REDACTED]

Laser Fusion Diagnostic Group

SHIVA DANTE SYSTEM TEMPORAL RESPONSE

During the recent 100-ps x-ray backlighting series on Shiva, the system temporal response was measured for both the mirror Dante (Dante M) and the 10-channel Dante S. Two gold disks were positioned at angles of 45° to the centerline of upper cluster of laser beams and were exposed to beams with intensities near $1 \times 10^{14} \text{ W/cm}^2$ and energies of about 300 J. The soft x-ray output of the gold disk was measured by the soft x-ray streak camera (SXRSC), an instrument with a temporal resolution of about 15 ps.

The averaged temporal response of the R7912 amplified channel had a FWHM of 731 ps; the direct-access Dante channels had an average FWHM of 335 ps, while a Dante channel using a TSN 660 French scope had a FWHM of about 209 ps.

The Dante Experiment

The Dante experiment is used by the laser program to provide spectral and temporal information about the low energy x rays emitted by targets of the Argus and Shiva lasers. The standard detector used for these measurements is the XRD-31 x-ray diode.

At the Shiva facility, the x-ray detectors are located about 2 m from the center of the target chamber, and the recording oscilloscopes are in the basement below the target chamber. About 30 ft of RG-214 cable and 90 ft of 1/2-in. Air Helix are used to carry the signals to the recording station.

At the recording station are 16 Tektronix 7912 transient digitizers (one for each channel) and one 4 GHz TSN 660 oscilloscope. The TSN 660 was teed into Dante M channel 4 for this experiment. Eight direct-access 7912s and eight amplified 7912s were used in the experiment.

Laser Fusion Diagnostic Group

Measurements

Several of the regular K- and L-edge x-ray absorption filters were replaced with 0.5- μm vanadium foils to give those detectors identical x-ray driving functions. The boron and carbon Dante M channels were not replaced with vanadium because the mirror cutoff energy on those channels is below 500 eV (the vanadium L edge).

Two gold disks, each tilted 45° with respect to the equator of the target chamber, were exposed to the Shiva beam. The Dante S was mounted on the equator, the Dante M was mounted 15° above the Dante S, and the SXRSC was mounted 15° above the Dante M. The SXRSC provided an accurate temporal characterization of the source with a temporal resolution of about 15 ps.

The Shiva laser was operated at a wavelength of 1.06- μm with a nominal pulse duration of 70 to 100 ps and was focused to an intensity of 10^{14} W/cm² with 300 J of energy delivered to the target. Figure 6 is a schematic of the experimental configuration.

Results

Figure 7 shows the x-ray driving function for a 500-eV x-ray channel as measured by the SXRSC. The driving function, which had a 106- to 113-ps FWHM, was removed from the measured data with the DCON frequency-domain deconvolution code.¹ The filter function, which controls the frequency cutoff for the unfold, was a super-Gaussian of form $\exp(-f^8)$ with 1/e cutoff frequencies of 6.25 GHz for direct-access scopes and 5 GHz for amplified scopes.

Figure 8 shows the averaged data for both shots on direct-access 7912s, and Fig. 9 shows the averaged results for amplified 7912s. The driving function was removed before the data were averaged.

Laser Fusion Diagnostic Group

Figure 10 shows the raw and unfolded data from the TSN 660 French scope. It is interesting to note that these results are similar to those reported by Lerche and Campbell.² These researchers did essentially the same measurement on the monojoule laser using an XRD-31 and a TSN 660 oscilloscope; the only difference is that the Shiva cable runs are much longer (120 ft as opposed to 30 ft) and the unfolded pulse width is correspondingly wider (209 ps as opposed to 140 ps).

Summary

The data presented here were derived from two shots that were sandwiched into a very busy shot schedule. The composite averages for the three types of channels (direct-access 7912, amplified 7912, and French scope) are adequate for unfolding data from target shots until better measurements can be made.

References

1. Feit, M., Users Guide to the DCON Deconvolution Code, UCID-18247 (1979).
2. Lerche, R. and Campbell, M., Temporal Response of the XRD-31, DDG 80-05 (1980).

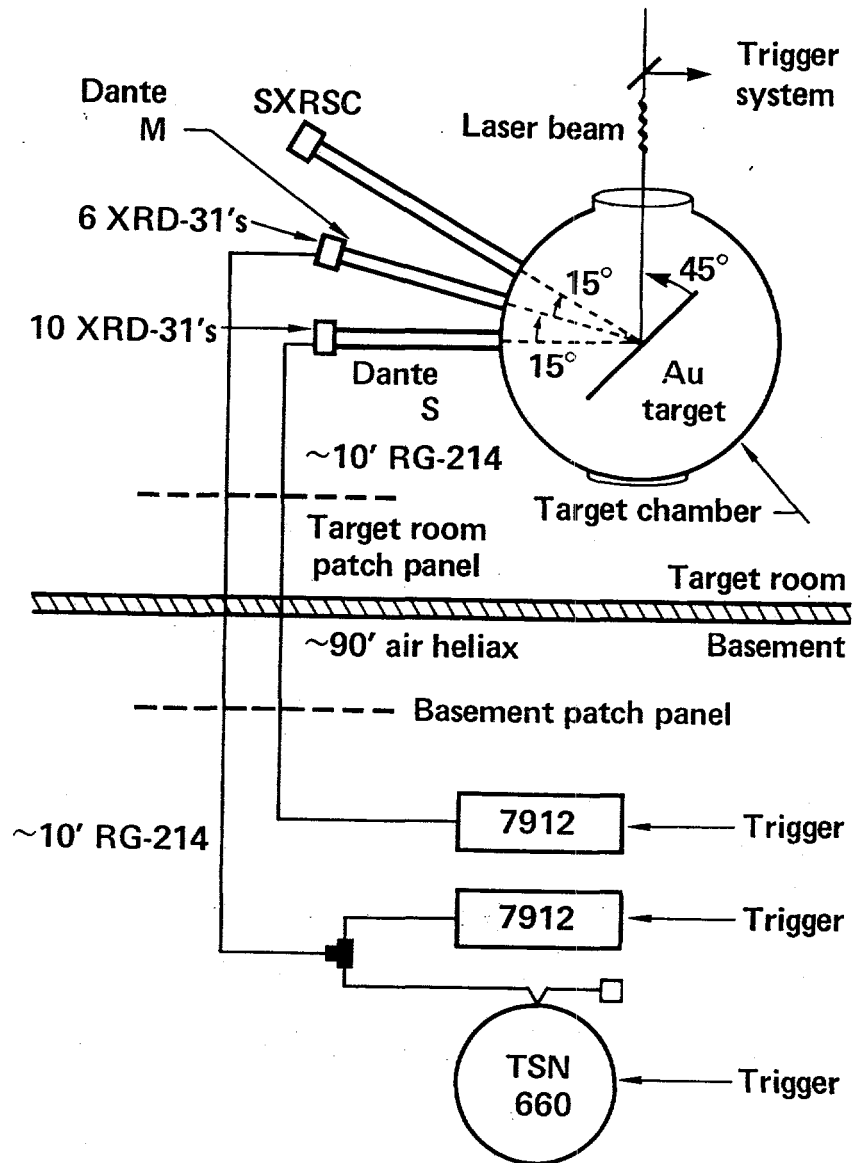
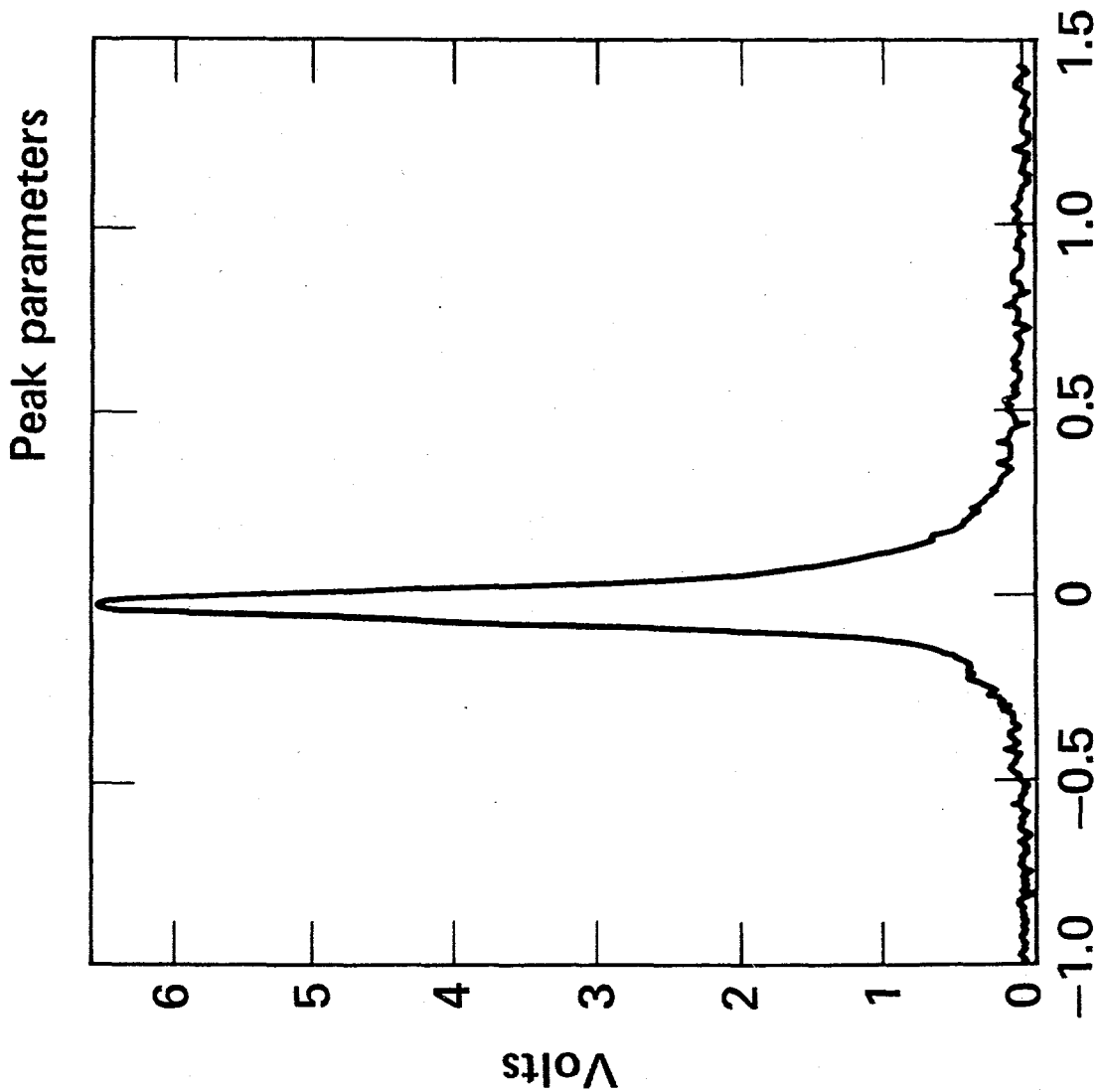


Fig. 6

Experimental Configuration

X-RAY DRIVING FUNCTION AS MEASURED BY STREAK CAMERA



Area: 1.000 V ns
Peak amp: 6.596 V
Risetime: 0.109 ns
Falltime: 0.136 ns
FWHM: 0.106 ns
-0.07 to 0.03 ns
FW 1/10 M: 0.284 ns
-0.14 to 0.14 ns
FW 9/10 M: 0.040 ns
-0.03 to 0.01 ns

20-50-0980-3113 Nanoseconds

Fig. 7

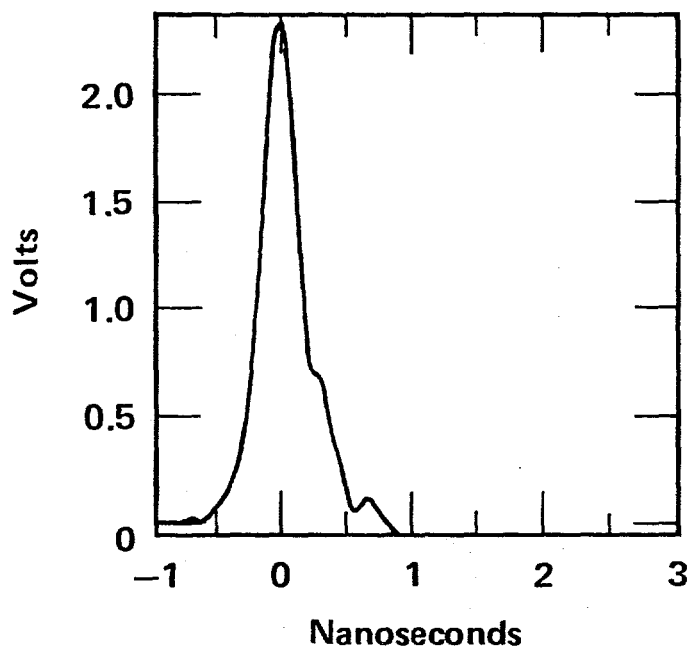
DIRECT ACCESS 7912-AVERAGED DATA, DRIVING FUNCTION REMOVED



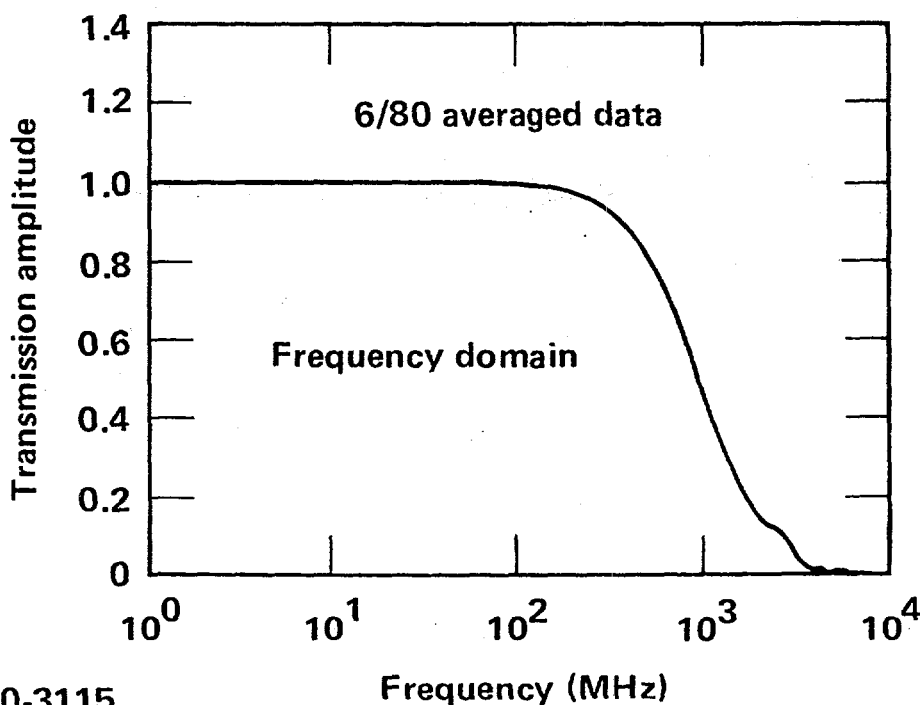
DANTE low energy x-ray data

Signals averaged over both shots and all channels

Peak parameters

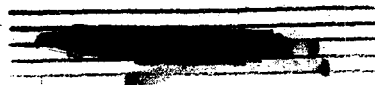


Area: 1.000 V ns
Peak amp: 2.369 V
Risetime: 0.306 ns
Falltime: 0.428 ns
FWHM: 0.335 ns
-0.18 to 0.16 ns
FW 1/10 M: 0.851 ns
-0.37 to 0.48 ns
FW 9/10 M: 0.117 ns
-0.06 to 0.05 ns



20-50-0980-3115

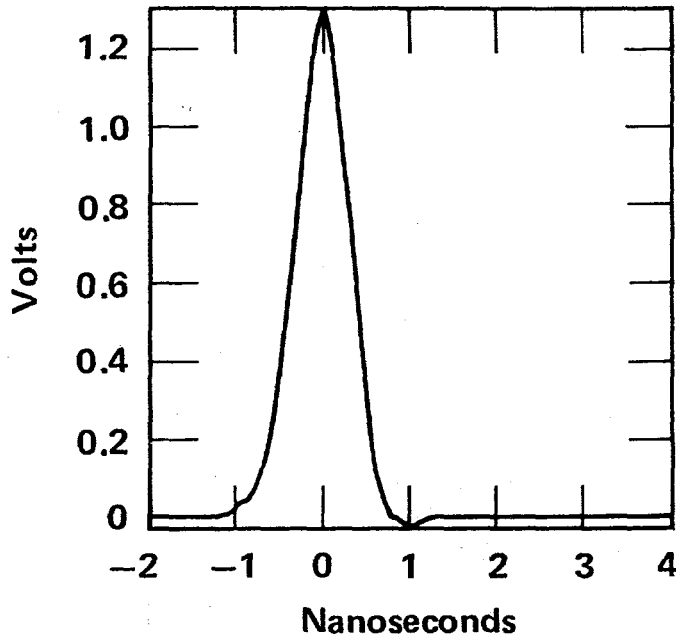
Fig. 8



DANTE LOW ENERGY X-RAY DATA SIGNALS AVERAGED OVER BOTH SHOTS AND ALL CHANNELS

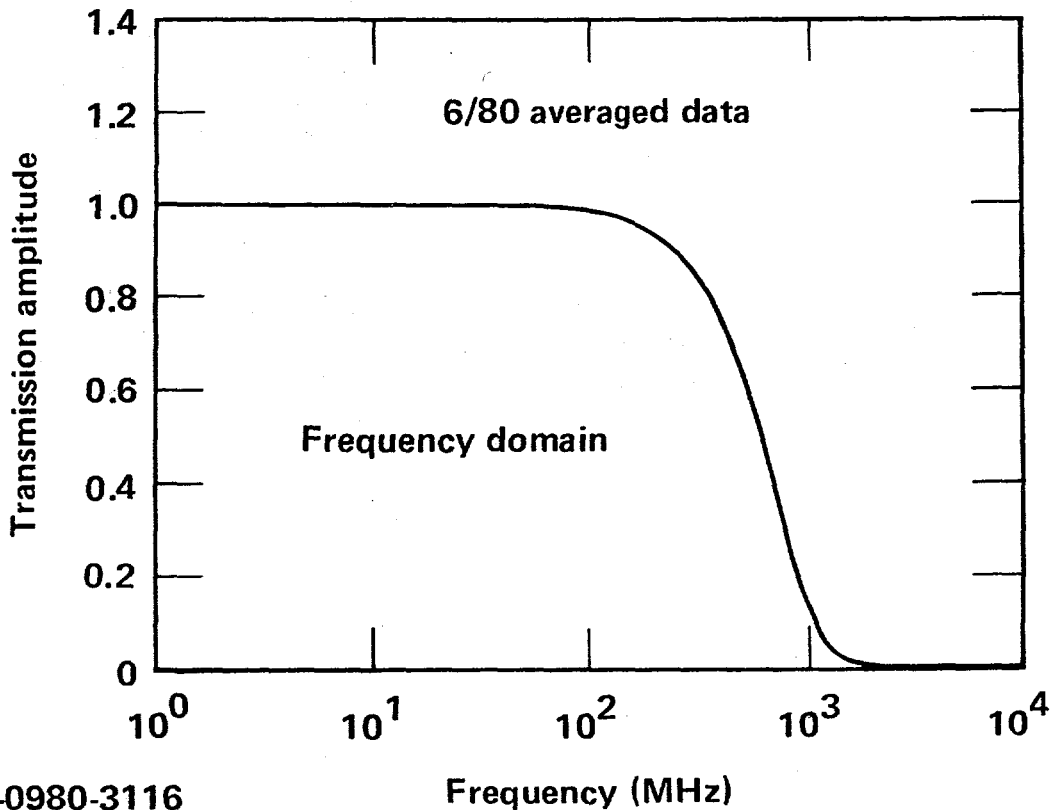


Peak parameters



Area: 1.000 V ns
Peak amp: 1.301 V
Risetime: 0.586 ns
Falltime: 0.505 ns
FWHM: 0.731 ns
-0.38 to 0.36 ns
FW 1/10 M: 1.344 ns
-0.71 to 0.63 ns
FW 9/10 M: 0.252 ns
-0.13 to 0.13 ns

Amplified 7912 averaged
data, driving function removed



20-50-0980-3116

Fig. 9

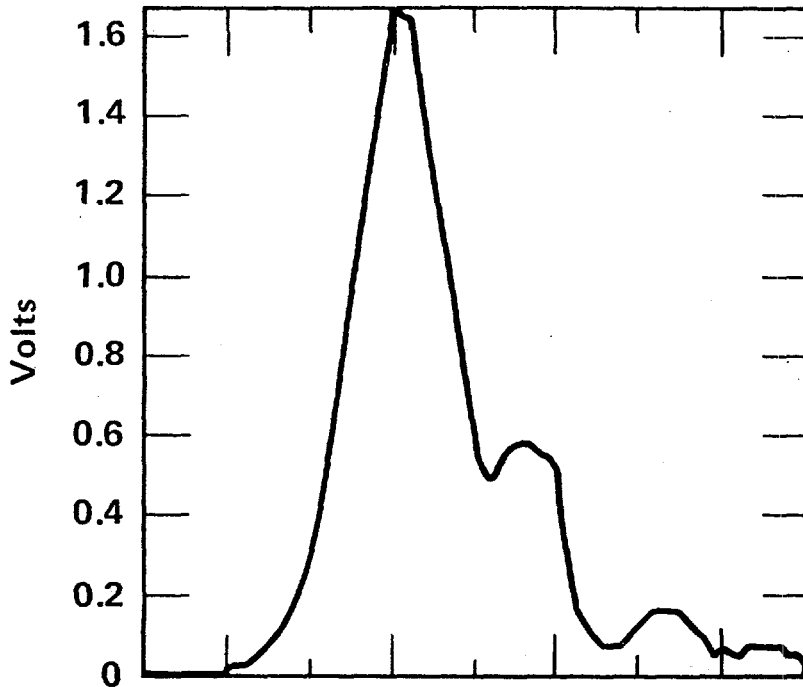


DANTE LOW ENERGY X-RAY DATA



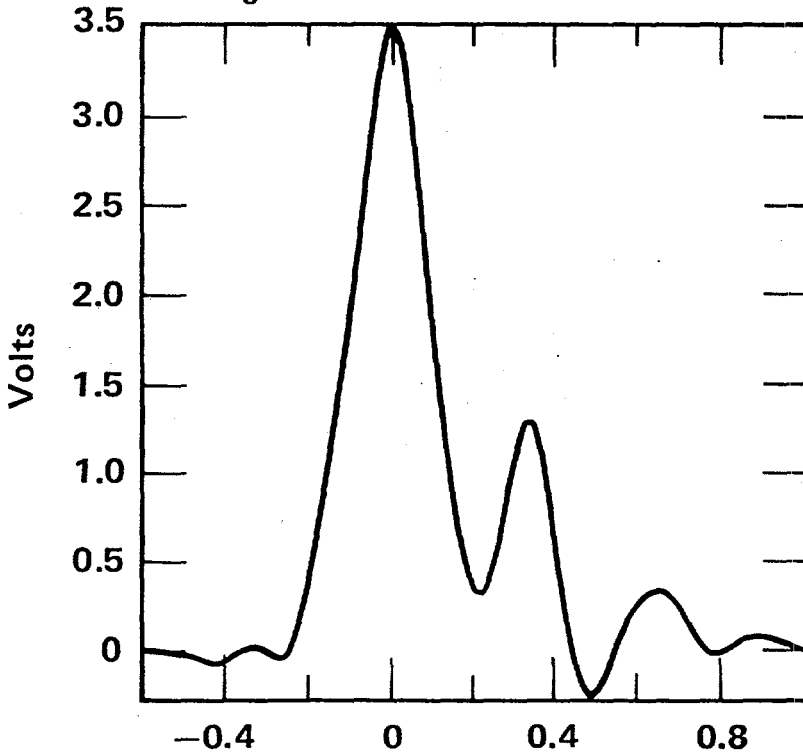
Peak parameters

Raw data



Area: 0.641 V ns
Peak amp: 1.669 V
Risetime: 0.219 ns
Falltime: 0.391 ns
FWHM: 0.281 ns
-0.12 to 0.16 ns
FW 1/10 M: 0.694 ns
-0.24 to 0.45 ns
FW 9/10 M: 0.084 ns
-0.03 to 0.06 ns

Driving function removed

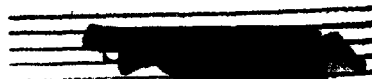


Area: 0.987 V ns
Peak amp: 3.532 V
Risetime: 0.171 ns
Falltime: -0.914 ns
FWHM: 0.209 ns
-0.10 to 0.10 ns
FW 1/10 M: -0.669 ns
-0.20 to -0.87 ns
FW 9/10 M: 0.075 ns
-0.03 to 0.04 ns

20-50-0980-3114

Nanoseconds

Fig. 10



Fusion Experiments and Analysis

 $2\omega_0$ EXPERIMENTS

Introduction

For laser-driven ICF to become a viable energy option, it is necessary to both maximize the fraction of the incident laser energy that usefully drives the implosion and minimize the fraction of the incident energy that (deleteriously) preheats the capsule. For several years, simulation calculations and a few limited experiments have indicated that short-wavelength lasers ($\leq 1 \mu\text{m}$) have a better potential as ICF drivers than do longer wavelength lasers ($\geq 1 \mu\text{m}$).^{1,2} Two schemes have been widely considered to drive ICF capsules: electron conduction in a uniformly illuminating geometry and soft x-radiation-heated implosions irradiated by two or more laser beams. Target design at LLNL has concentrated on the latter for a number of reasons. Targets driven with soft x-rays have a higher calculated gain for reactor size targets than do similarly driven direct illumination targets. Since the driving radiation is produced in the wall of a case several capsule radii from the capsule, nonuniformities in the driving conditions due to beam modulations and beam discreteness is very effectively smoothed. This is very important because of the large convergence ratio required for high performance targets. Also by adjusting the material opacity and the driving temperature to control density gradients, we can greatly reduce sensitivity to fluid instabilities relative to directly illuminated targets. We also emphasize the radiation driven targets because there is no known viable reactor design approach for "uniform illumination" electron conduction driven targets.

Argus and Shiva, have been able to drive small, high-Z radiation cases to equivalent black-body temperatures of almost 200 eV (see Ref. 3). However, radiation cases if driven to too high a temperature

Fusion Experiments and Analysis

also display an undesirably large "hot" electron preheat flux,³ far exceeding that observed when the same amount of laser energy irradiates a disk target. This production of very energetic (and therefore penetrating) electrons depends on a number of processes, all of which are, to some extent, dependent on laser wavelength.

Early this year, wavelength-scaling experiments with $\lambda = 0.532 \mu\text{m}$ light were undertaken using the Argus laser facility with the following objectives:

- o Determine the absorption and scattering of 0.532- μm wavelength light by Au, Be, and CH targets as a function of incident intensity at ~600-ps pulse duration.
- o Measure the x-ray conversion efficiency in the range $0.1 \text{ keV} \leq h\nu \leq 100 \text{ keV}$ for the same target-irradiation conditions mentioned above.
- o Examine the performance of the Heinz B unity-aspect-ratio classified cylindrical radiation case (i.e., absorption, drive and preheat) with available laser energy.

At this writing, the experimental measurements are complete, data analysis is well underway, and some of the results are outlined below.

Fusion Experiments and Analysis

Table 1
Experimental Conditions

Incident Energy at $\lambda = 0.532 \mu\text{m}$	5 - 40 J
Pulse Width (FWHM)	~600 ~700 ps
Focusing Optics	f/2
Spot Size (diameter)	~180 μm (3×10^{13}) 180 μm , 80 μm (3×10^{14}) ~80 μm , (10^{15}) ~30 μm ($\geq 3 \times 10^{15}$)
Beam Modulation (Peak/Average)	~3:1
Target Materials	Au, Be and CH disks and Au cylinders
Target dimensions	
Disks:	600 μm in diameter and 14 to 25 μm thick
Heinz B Au cylinders:	0.4 scale with a diameter of 200 μm , 200 μm long, and with one 100- μm -diameter pinhole 0.6 scale with a diameter of 300 μm , 300 μm long, and with one 150- μm -diameter pinhole

Fusion Experiments and Analysis

In May we reported preliminary results of our absorption measurements using an enclosing box calorimeter.³ Table 1 summarizes the experimental conditions for these measurements, and Fig. 11 gives the central results. High-Z targets show satisfyingly high absorptions over the entire range of intensities of interest in current ICF target designs. These data suggest that most of the 0.532- μm laser energy would be absorbed on the first bounce in a radiation case. Indeed, when two 0.4-scale Heinz B cylinders and two 0.6-scale Heinz B cylinders were irradiated, their absorptions were $\geq 90\%$. It should be remembered, however, that efficient absorption has never been a problem with 1.06- μm -irradiated hohlraum targets. Typical classified CAIRN target absorptions have been $\sim 80\%$ for both Argus- and Shiva-scale assemblies. The hoped-for improvements in target performance arise from anticipated gains in soft x-ray conversion efficiency coupled with reduced suprathreshold electron production; nevertheless, confirmation of high target absorption was gratifying.

X-RAY CONVERSION EFFICIENCY AND SUPRATHERMAL X-RAYS

After the conclusion of the absorption study, the box calorimeter was removed from the Argus target chamber and preparations for x-ray conversion measurements were begun. Figure 12 shows the locations of the major x-ray measuring instruments on the Argus target chamber. Of course, the Argus chamber is actually cylindrical with the 0.532- μm laser beam entering the chamber from the south, but it is represented here as a sphere to emphasize the spherical coordinates of the diagnostics. When a planar disk target is placed at the center of the chamber and its normal is rotated in the polar angle θ holding $\phi = 90^\circ$ and constant, it presents different points of view to each of these

Fusion Experiments and Analysis

instruments. The three DANTE low-energy spectrometers and the fast flat calorimeter, mounted in FFLEX, are primary diagnostics for measurements of soft x-ray conversion efficiency.⁴ Figure 13 shows the viewing angles for these instruments for the three target normal polar angles used, +30°, +10° and -30°. Because the targets were irradiated with an $f/2.2$ lens, the absorption did not vary within a measurement accuracy of $\pm 5\%$ for target rotations of $\pm 30^\circ$. Given the fact that target absorption is independent of θ for these "near normal" irradiations and assuming that the soft x-ray emission from the disk target is azimuthally symmetric about its normal, the instruments (positioned as shown in Fig. 12) provide eight distinct and well-spaced viewing angles with respect to the target normal. In addition, the -30° orientation provides a check of the azimuthal symmetry assumption since both DANTE L and DANTE W view the target from the same angle, β_n , but widely different azimuthal angles.

The data collected on the angular distribution of soft x-ray emission from Au irradiated at $I \sim 3 \times 10^{14}$ W/cm² are presented in Figure 14. Similar data was collected for $I \sim 3 \times 10^{13}$ W/cm² and $I \sim 3 \times 10^{15}$ W/cm². A Lambertian emitter would have an angular distribution proportional to $\cos \beta_n$ and appear as a straight line extending diagonally from the origin in Fig. 14. An Au disk heated by 0.532 μm light gives rise to an x-ray emitting plasma that expands away from the disk surface at a velocity of order 10^6 cm/s. The x-ray angular distribution recorded is thus neither purely Lambertian (static disk emitter), nor is it isotropic (expanding spherical plasma).

To determine the total x-ray yield, the angular distribution of the emission must be summed over 2π steradians and integrated over the energy interval 0.1 to 1.5 keV. Figure 15 compares the total x-ray yield with LASNEX simulation calculations for Au. While substantial

Fusion Experiments and Analysis

uncertainties persist in the exact target irradiation peak intensities, the reduction in x-ray conversion efficiency observed at $I \sim 10^{13} \text{ W/cm}^2$ disagrees with the simulations to an extent that exceeds experimental error. Both the data reduction and the simulation calculations are, therefore, under review. The energy loss channels available to the plasma are radiation, electron thermal conduction and hydrodynamic. The observed high absorption, apparently due to classical collisional processes, argues against high plasma ion temperatures and the accompanying large hydrodynamic loss rates. Fundamentally, a target irradiated with a lower laser-power density should produce a reduced spatial temperature profile with a lowered x-ray emission; however, the measured reduction in emission efficiency at $I \sim 10^{13} \text{ W/cm}^2$ falls below LASNEX numerical simulation. The data now in hand reveal that x-ray conversion efficiencies of 50% at $I \sim 3 \times 10^{14} \text{ W/cm}^2$ --well above those measured for corresponding $1.06 \mu\text{m}$ target irradiations--can be routinely obtained.

In order to assess the relative effectiveness of $0.532\text{-}\mu\text{m}$ target irradiations in producing suprathermal electrons, the suprathermal x-ray spectrum was monitored using a filter-fluorescer spectrometer on every target shot.⁵ We interpret a smaller suprathermal x-ray flux to mean a reduction in suprathermal electrons production and hence a lower "hot" electron preheat. Figure 16 is a compilation of x-ray spectra measured from the Au targets tested. As in short-pulse $1.06\text{-}\mu\text{m}$ target irradiations, the slope of the suprathermal x-ray spectrum, θ_H , increases with increasing power density approximately according to $(I\lambda^2)^{0.4}$. Also, as in $1.06\text{-}\mu\text{m}$ -heated classified target irradiations, the suprathermal x-ray flux from the Heinz B targets was high in comparison with Au disks. No exactly comparable radiation cases have yet been irradiated with $1.06\text{-}\mu\text{m}$ pulses,

Fusion Experiments and Analysis

but hohlraum-scaling studies performed on similar cylindrical targets at Shiva revealed the following empirical scaling relationship for the suprathreshold x-ray flux at 50 keV from 1.06- μ m-heated targets:

$$I_{50} = 5.2 \times 10^{15} \left(\frac{E \text{ (kJ)}}{S^3} \right)^3 \text{ keV/keV}^3$$

Both of the Heinz B targets ($S = 0.6$ and 0.4) were irradiated by 30 ± 3 J in 700 ps and, as can be seen in Fig. 16 and from the empirical scaling, their suprathreshold x-ray flux is between 500 and 700 times lower than correspondingly scaled 1.06- μ m experiments. If this dramatic reduction in suprathreshold x-ray flux indeed reflects a corresponding reduction in hot-electron preheat, significantly improved target performance should be possible with a frequency-doubled Nd: Glass driver. Further tests of these preliminary findings await the performance of an exactly comparable 1.06- μ m experiment and several kilojoule 0.532- μ m hohlraum-scaling studies.

Several mechanisms might produce these suprathreshold x-rays, and their relative contributions are poorly understood. Resonance absorption gives rise to hot electrons whenever high laser intensities approach the critical electron-density surface.⁶ Argus 0.532- μ m laser beams contain substantial modulation so that a range of intensities is incident on the target. In order to quantify the intensity range impinging on the targets, equivalent-target-plane photographs were densitometered and energy-distribution functions plotted (such as that shown in Figure 17). Even though the target was irradiated at a nominal intensity of $2\text{-}3 \times 10^{14}$ W/cm², about 5% of the incident beam energy reached the target at 10^{15} W/cm². This small fraction of the energy reaching the target at elevated intensities may produce the bulk of the

Fusion Experiments and Analysis

very-high-energy electrons responsible for suprathreshold x-ray flux at 50 keV. Since the Heinz B targets were aligned so that the best focus of the f/2.2 lens was at the center of the pinhole, the beam diverged into the cavity. For example, the 0.4-scale Heinz B hohlraum back wall was irradiated with about 5×10^{14} W/cm². Figure 16 shows that the suprathreshold x-ray flux detected from this target lies about a decade above an Au disk irradiated with $1-2 \times 10^{15}$ W/cm². It is not impossible that the increased surface area of the classified target, together with refractive effects in the blow-off plasma, might account for the higher suprathreshold x-ray flux.

Stimulated Raman Scattering

In addition to the high-energy x-ray diagnostics, an array of filtered photodiodes looked at the Raman-scattered light near 1.06 μ m. They showed that the Raman instability went vigorously in the 200- μ m hohlraum; about 5×10^{-3} of the incident laser energy was detected as Raman-scattered light emerging from the pinhole. For the 0.6 scale hohlraum, only about 2.5×10^{-4} of the incident laser light emerged as Raman light. The high-energy x-rays were down by about the same factor. The amount of Raman light emerging from the 0.4 Cairn was 100 to 1000 times greater than the Raman light generated by a disk target irradiated with the same energy at an intensity of $1-2 \times 10^{15}$ W/cm².

Figure 18 shows the spectrum of the Raman light scattered from an 0.4 scale Heinz B target both in and out of the plane of polarization of the incident laser beam. The spectrum of the Raman light was peaked between 850 and 900 nm with a bandwidth of ~ 150 nm. Light at this frequency is expected for the Raman backscatter instability at about $0.10 \times$ critical density.⁷ This puts a lower bound on the level of Raman scattering

Fusion Experiments and Analysis

occurring because an angular spread of the backscattered light will prevent the light from escaping from the hohlraum if it is produced far from the entrance hole. Also Raman backscatter near quarter critical will produce a backscattered photon very near its critical density and these photons will be strongly absorbed.⁷

The photodiodes were prevented from seeing the 0.532- μm laser light by Schott RG-610 sharp red cut-on color filters. The interference filters were fully blocked to optical density 4 and had a nominal peak transmission of 55-60% and a nominal bandwidth of 12.5 nm FWHM. X rays were shielded against by lead-glass windows of 3-mm lead-equivalent thickness and tungsten alloy housings. Some diodes were always prevented from detecting light either by being covered with aluminum foil or by using a very high value for the neutral-density filter. The x-ray background was always too low to be detected.

A solid angle of 1.5 to 2 steradians was measured by another array of photodiodes equipped with dielectric filters that were highly reflective at 1.064 μm (instead of the normal band-pass interference filters). The spectral region 610 to 900 nm was transmitted. The 1.064- μm reflective dielectric filter was necessary because of the large amount of 1.064- μm light hitting near the target (in addition to the 0.532- μm light). The beam dump located beyond the frequency-doubling crystal transmitted about 10% of the 1.064- μm light, and all the subsequent turning mirrors were highly reflective at 1.064 μm , as well as at 0.532 μm . About 20-30% of this 1.06- μm light was focused within a few mm of the target. Our detectors were therefore protected against this noise source.

As noted in earlier issues of this Monthly, stimulated Raman scattering (light wave converts into two electron plasma waves) results in high-phase-velocity electron plasma waves. Landau damping of

Fusion Experiments and Analysis

these waves may result in the production of very-high-energy suprathermal electrons.^{3,8,9} These processes occur at plasma densities of $1/4 N_c$ or less, making them likely candidates in the plasma-filled hohlraums. The fraction of the suprathermal electron production attributable to these processes is not known quantitatively at this time, however.

Summary

Efficient laser light absorption was observed for incident intensities between 10^{13} W/cm² and 10^{16} W/cm². Approximately 50% of the energy absorbed by Au plasmas irradiated by $\sim 3 \times 10^{14}$ W/cm² was emitted as subkilovolt x rays. Suprathermal x-ray fluxes from classified targets fell well below scaled 1.06- μ m results. Raman scattered light, a signature of one important preheat producing process, was detected. The prospects for 0.532- μ m-heated soft-x-ray driven targets are favorable.

Fusion Experiments and Analysis

References:

1. C. E. Max and K. G. Estabrook, "Wavelength Scaling in Laser Fusion from a Plasma Physics Point of View", Lawrence Livermore National Laboratory, Livermore, Calif., UCRL-82671 (1979).
2. E. Fabre, et al., 1979 APS Meeting, Division of Plasma Physics, Boston, Mass.
3. See for example: "Laser Fusion Monthly Report", MM 80-5, May 1980.
4. K. G. Tirsell, H. N. Kornblum, and V. W. Slivinsky, "Time Resolved, Sub-keV X-Ray Measurements Using Filtered X-Ray Diodes", Lawrence Livermore National Laboratory, Livermore, Calif., UCRL-81478, (1979).
5. B. L. Pruett, K. G. Tirsell, H. N. Kornblum, S. S. Glaros, D. E. Campbell, and V. W. Slivinsky, "A Ten Channel Filter-Fluorescer Spectrometer", Lawrence Livermore National Laboratory, Livermore, Calif., UCRL-81477, (1978).
6. K. G. Estabrook, E. J. Valeo, W. L. Kruer, "Phys. Fluids", 18, 1151, (1975).
7. D. W. Phillion, "Observation of Raman-Scattered Light in 1.06 μm Laser-Irradiated Plasmas", Lawrence Livermore National Laboratory, Livermore, Calif., UCRL-84148 (1980).
8. W. L. Kruer, K. G. Estabrook, B. F. Lasinski, and A. B. Langdon, "Raman Backscatter in High Temperature Inhomogenous Plasmas", Lawrence Livermore National Laboratory, Livermore, Calif., UCRL-82394 (1979).
9. A. B. Langdon, B. F. Lasinski, and W. L. Kruer, "Phys. Rev. Lett.", 43, 133, (1979).

EFFICIENT ABSORPTION AT LOW INTENSITY IS CONFIRMED BY RECENT EXPERIMENTS WITH 0.5 μ LIGHT

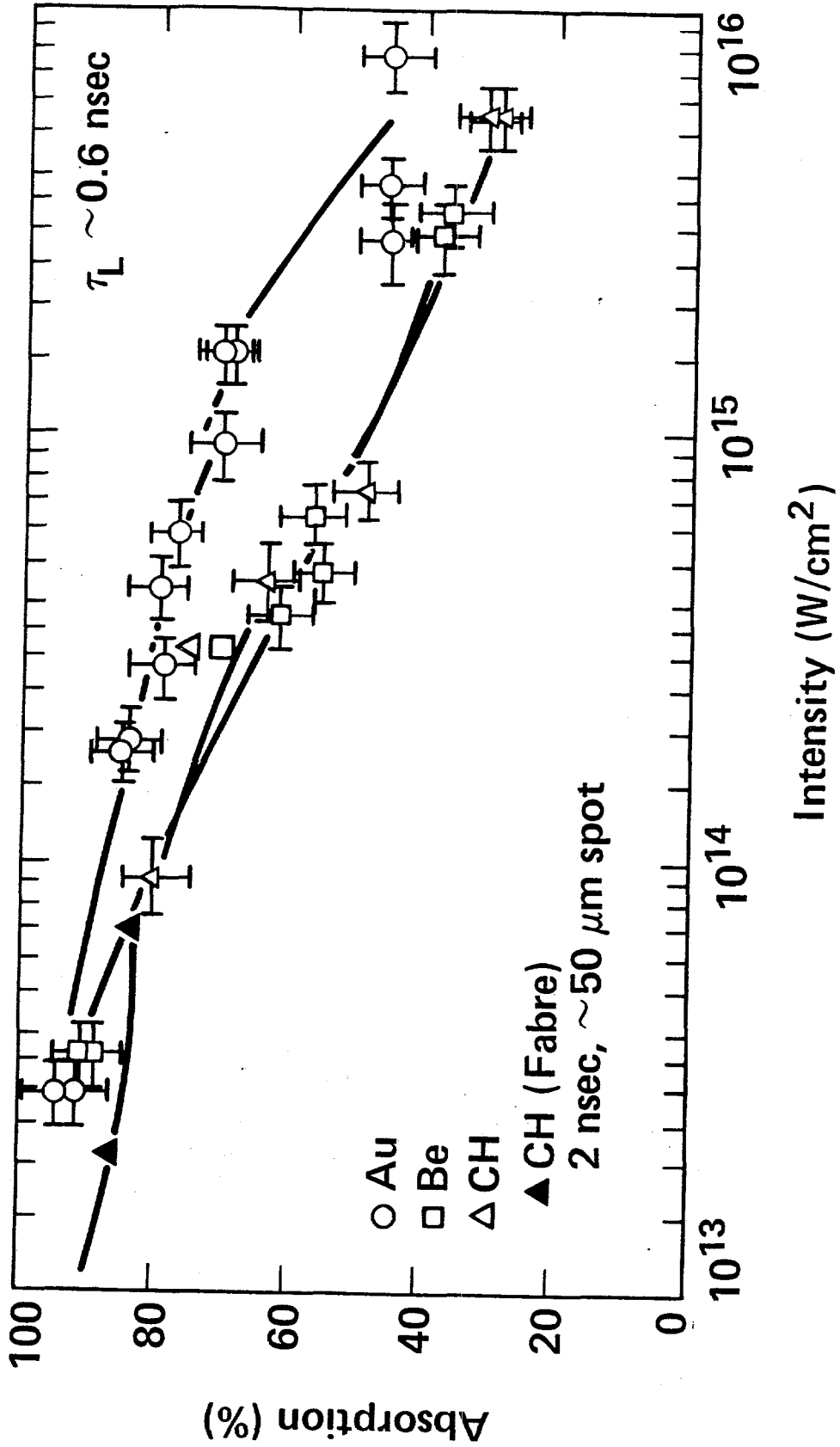


Fig. 11

LOCATIONS OF THE MAJOR X-RAY MEASURING DIAGNOSTICS ON THE ARGUS TARGET CHAMBER

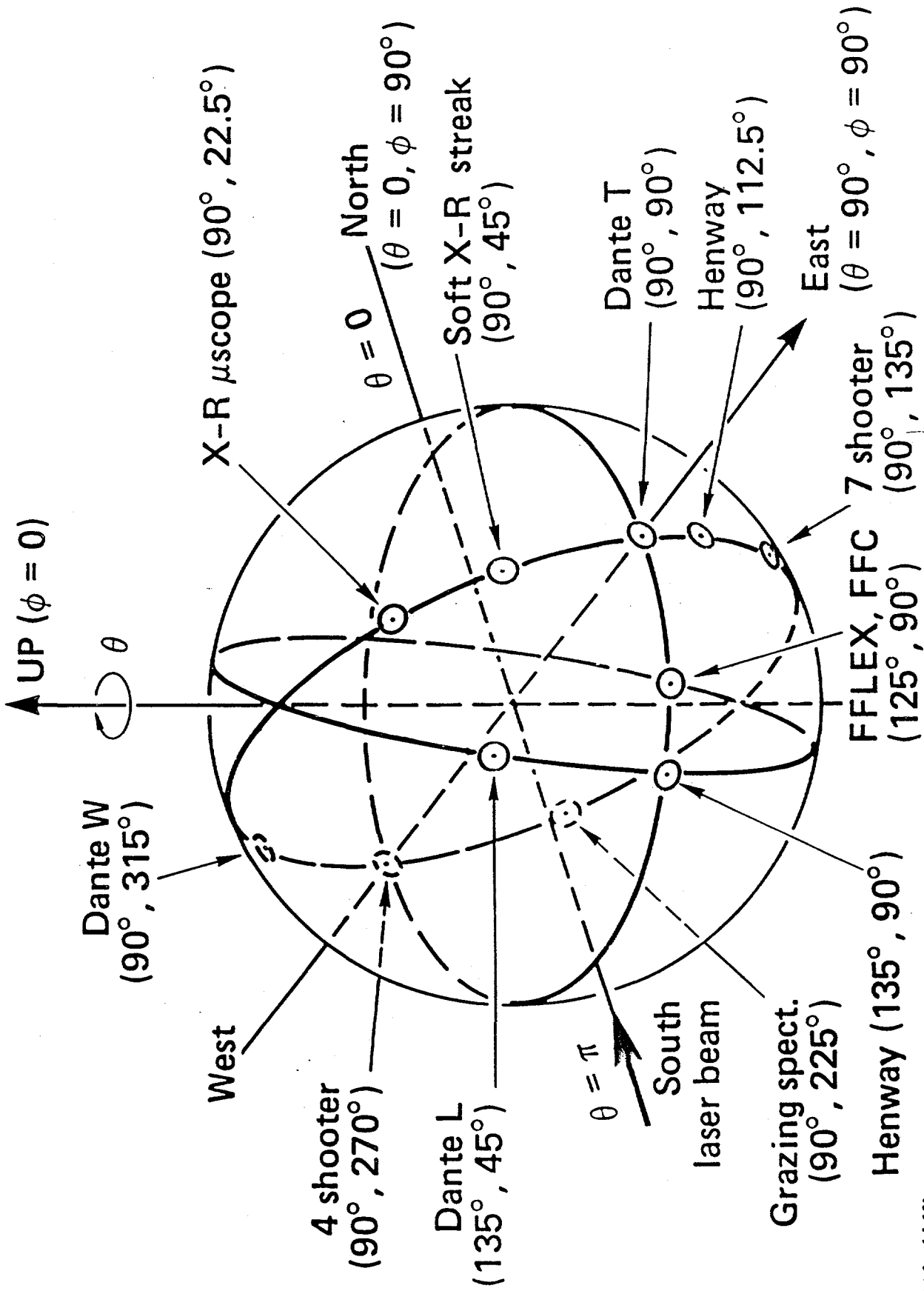


Fig. 12

*This page intentionally
left blank.*

SOFT X-RAY DIAGNOSTIC VIEWING ANGLES

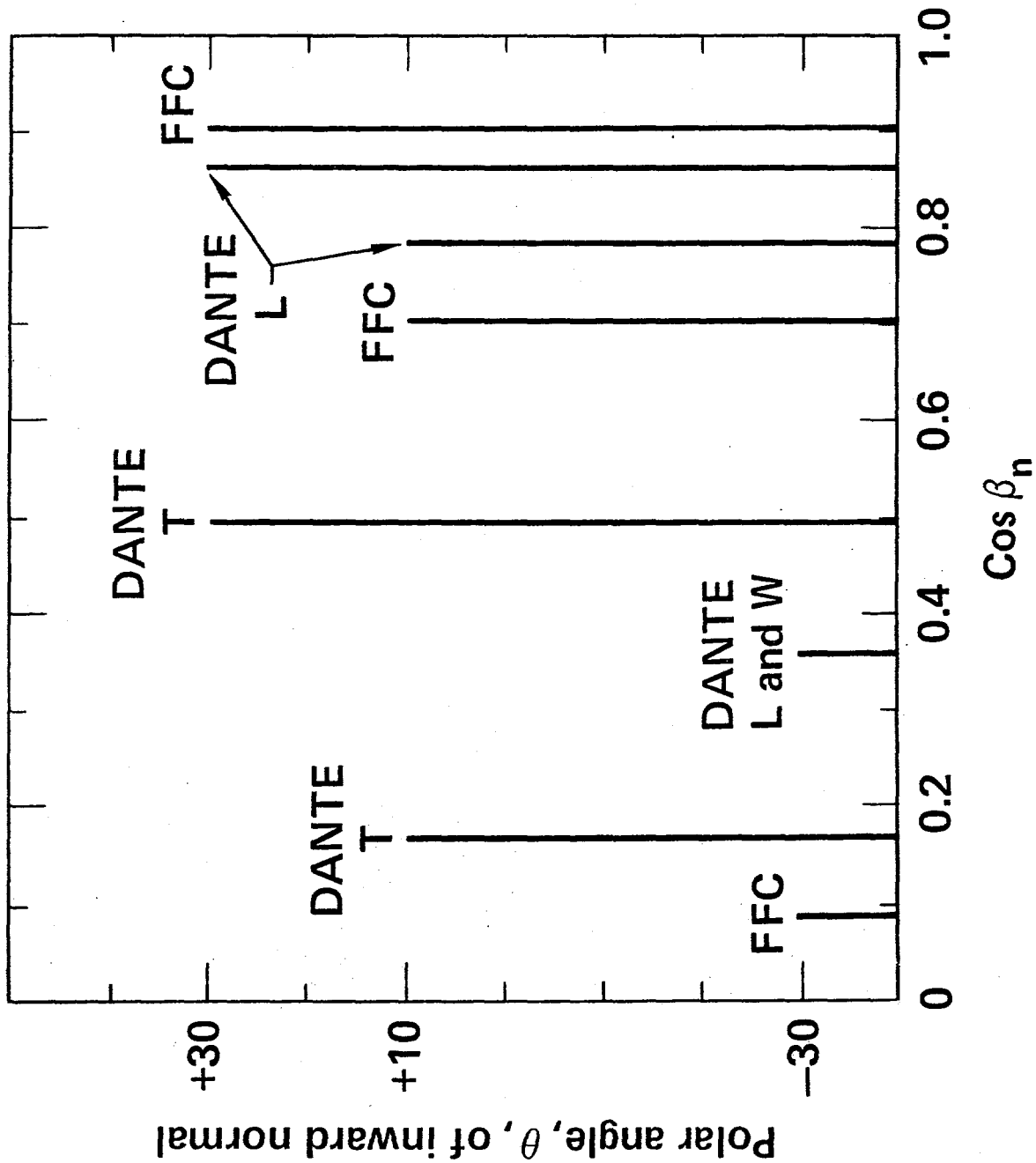


Fig. 13

ANGULAR DISTRIBUTION OF X-RAY EMISSION FROM Au AT
 $I \sim 3 \times 10^{14} \text{ W/cm}^2$ (25 Joules/600 psec)

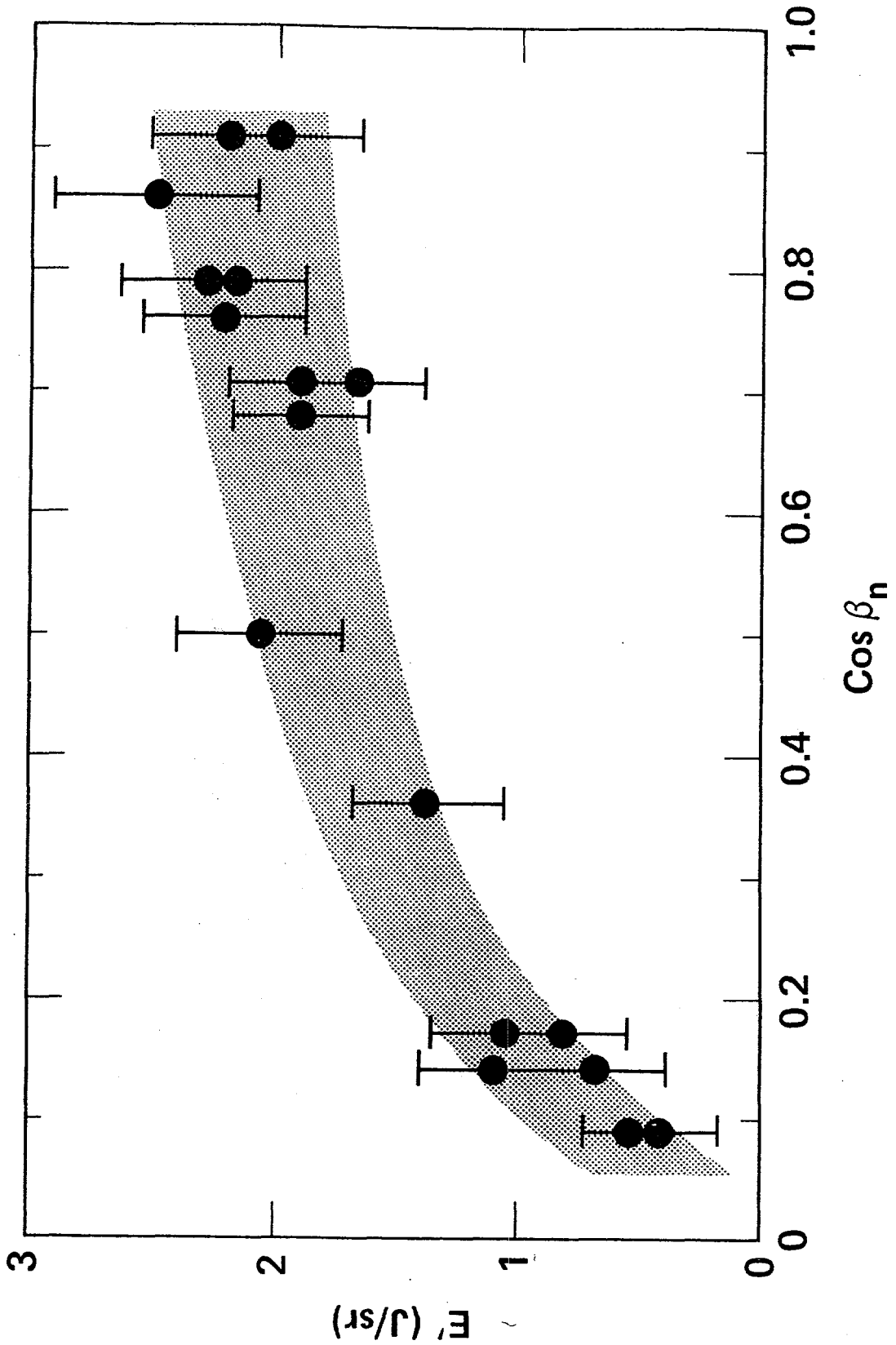


Fig. 14

SOFT X-RAY CONVERSION EFFICIENCY EXPERIMENTAL
RESULTS AND CALCULATIONS FOR $\lambda_L = 0.532 \mu\text{m}$ AND

$\tau_L \approx 600 \text{ psec}$

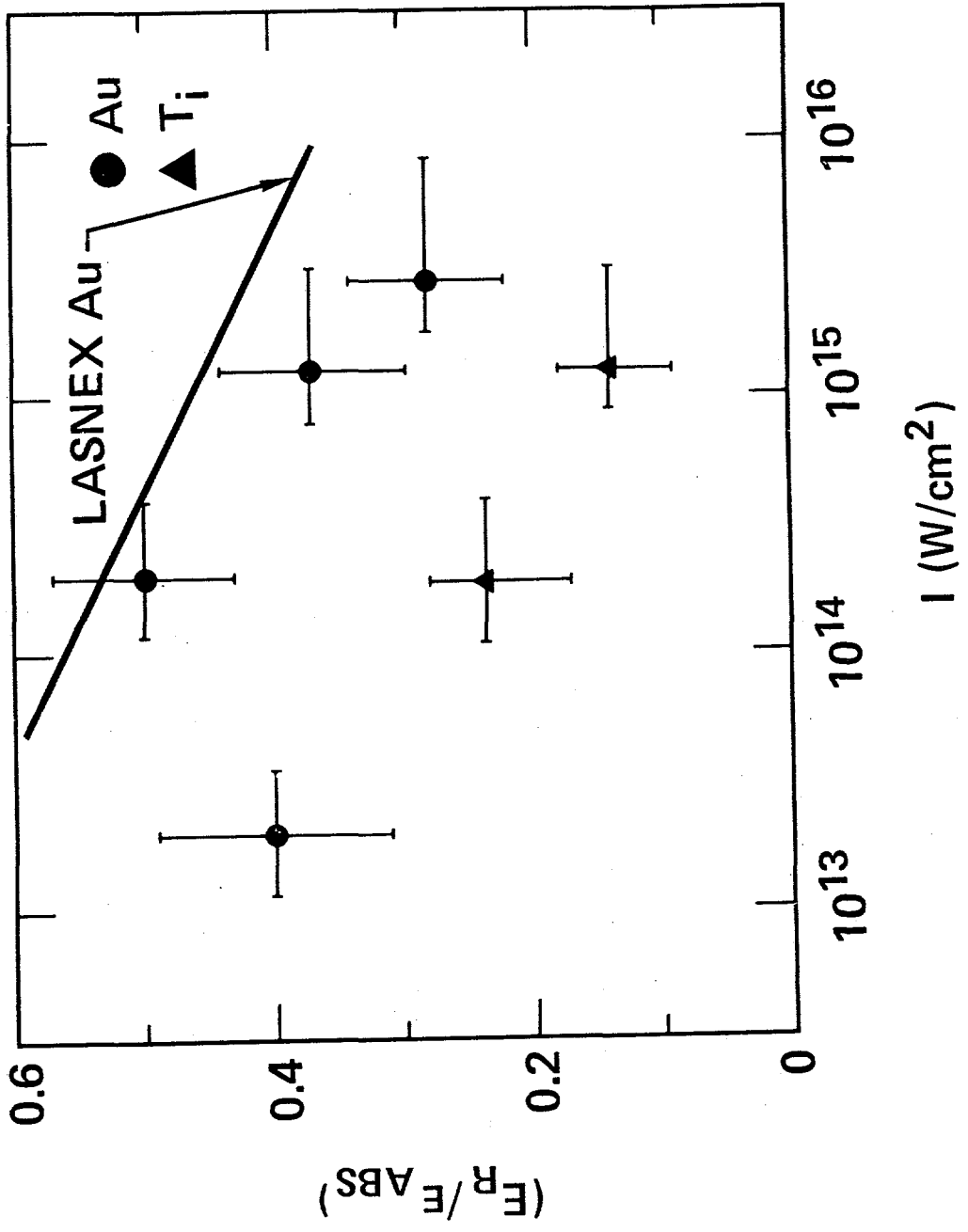


Fig. 15

SUPRATHERMAL X-RAY FLUX FROM Au TARGETS

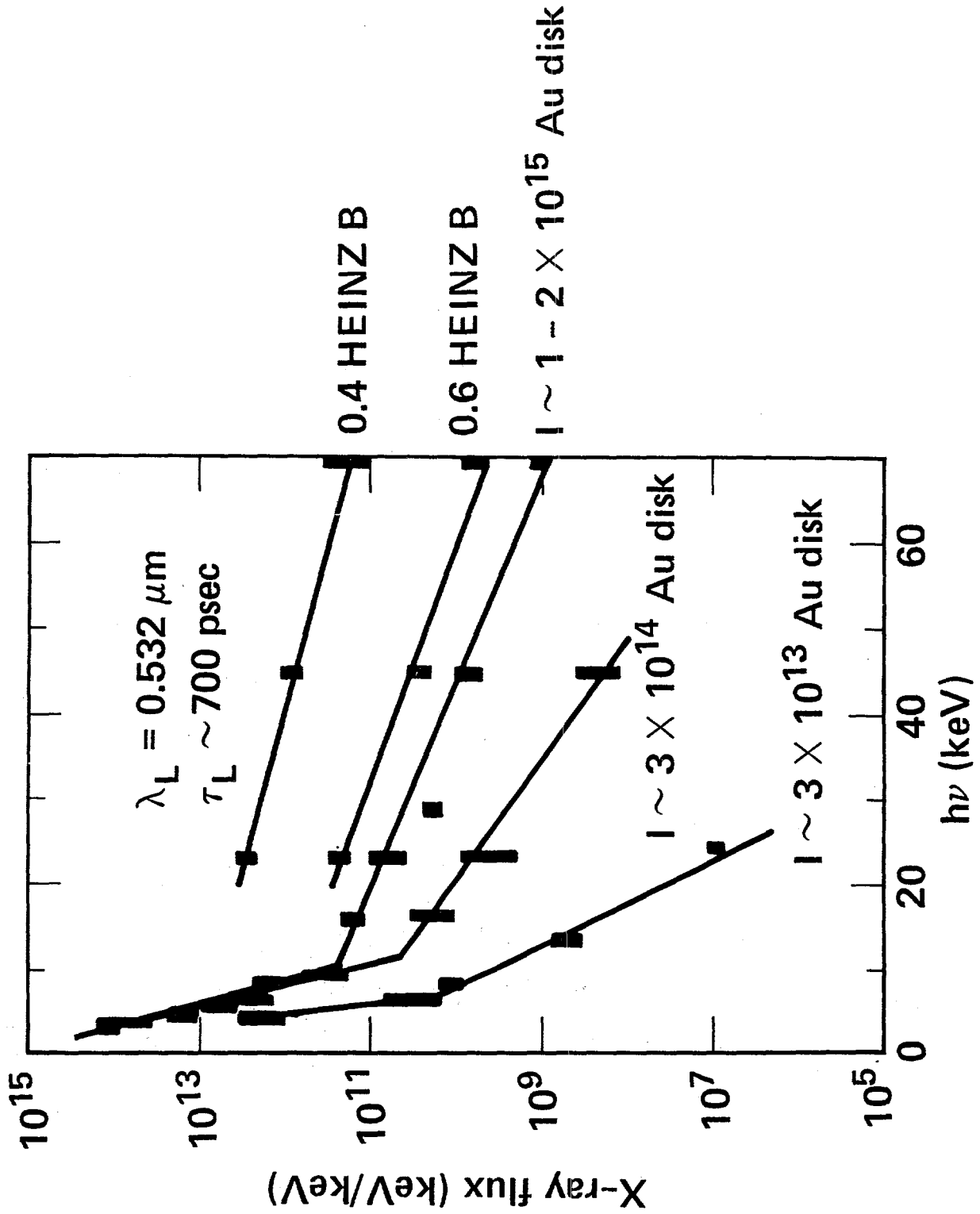


Fig. 16



Beam modulation

At a nominal intensity of $2-3 \times 10^{14} \text{ W/cm}^2$
 $\sim 5\%$ of the incident beam energy is at $\sim 10^{15} \text{ W/cm}^2$

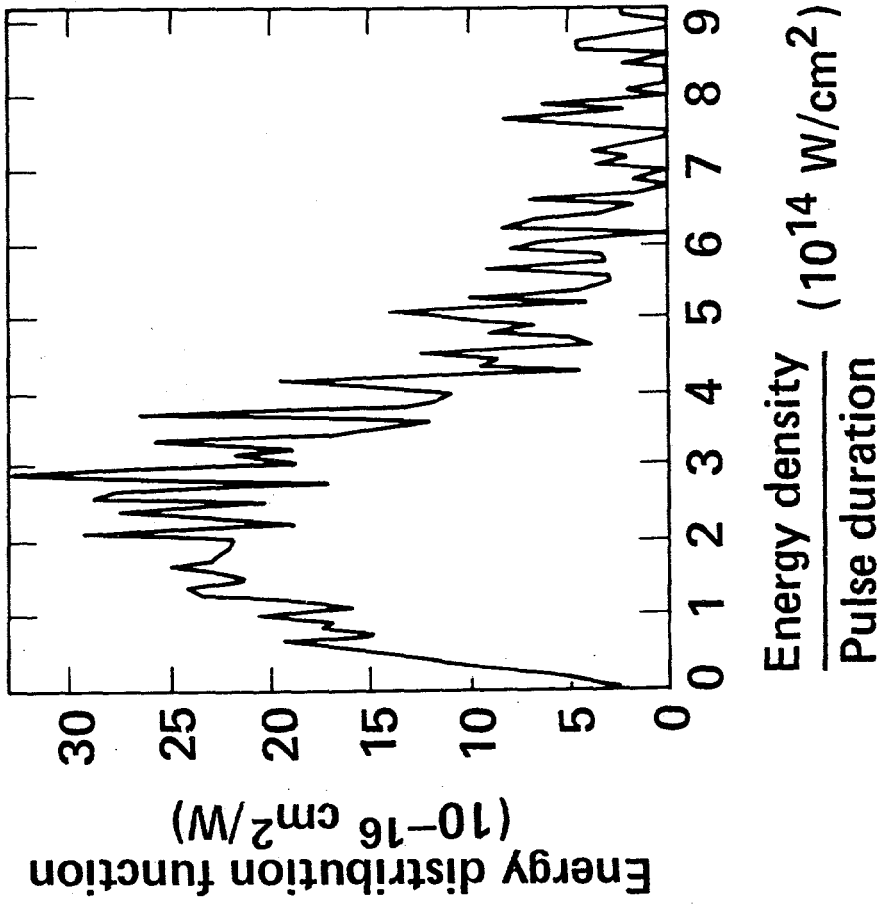


Fig. 17

*This page intentionally
left blank.*

THE RAMAN INSTABILITY GOES VIGOROUSLY FOR 25J GREEN LIGHT IN A 0.4 SCALE HEINZ B TARGET

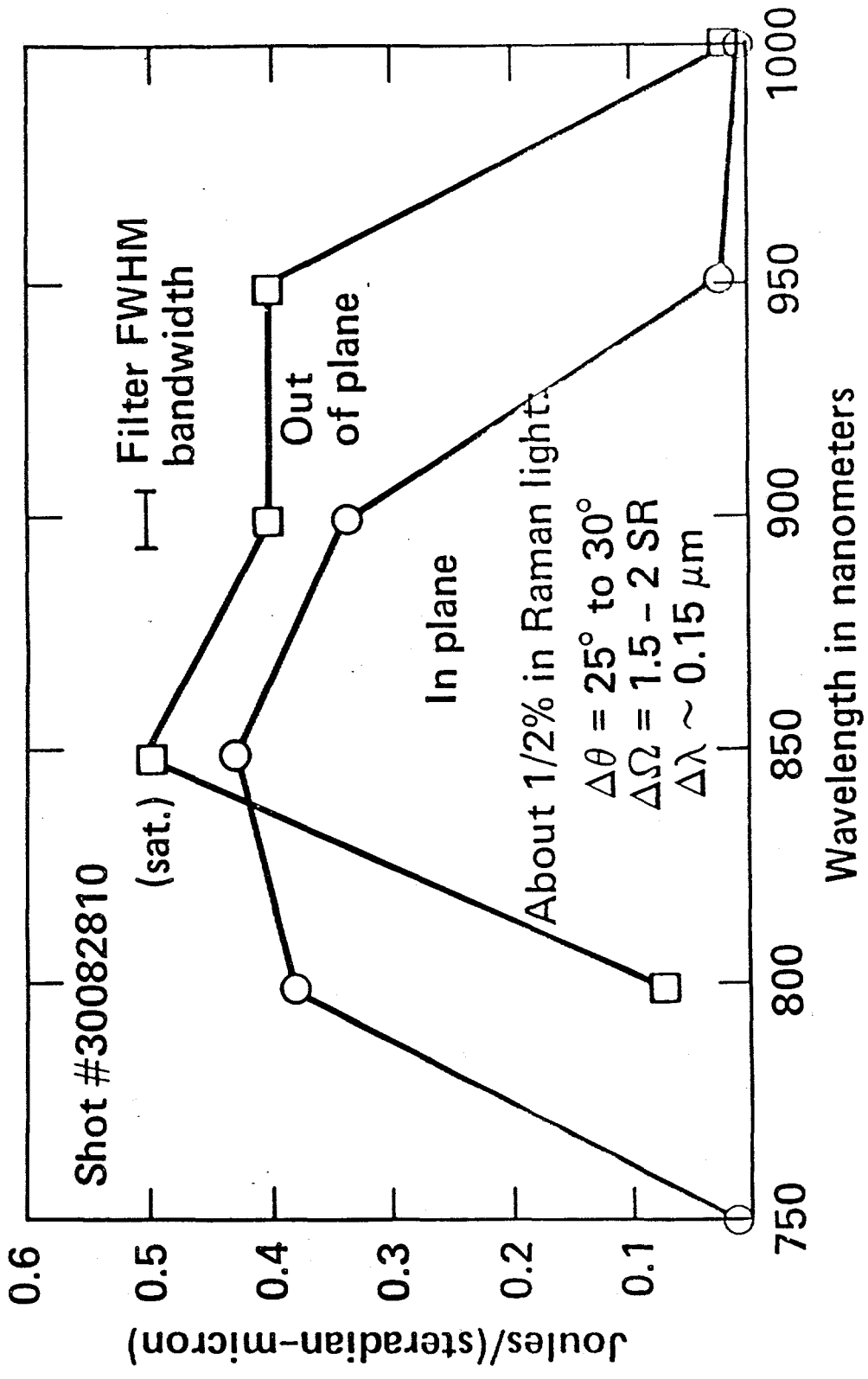


Fig. 18

*This page intentionally
left blank.*

Energy Applications R&D

PLANNING FOR AN ENGINEERING TEST FACILITY

Introduction

The engineering development required to harness energy output from inertial confinement fusion (ICF) is currently being addressed on a very small scale. However, experience with the development of other new technologies indicates that a substantial engineering-development time will be required for ICF energy-conversion systems.

To begin planning such a development program, we invited representatives from much of the ICF reactor community* to LLNL in July to define an ICF engineering test facility (ETF) and to discuss the reactor technology development that will be required before the ETF can become a reality. This meeting was notable for the spirit of cooperation and for the agreement on technical issues, and the more important discussions of the meeting are summarized in this report.

Design Goals and Issues for the ETF

The following design goals and issues were established as being of paramount importance for developing the ETF:

o There must be systems integration of all the major ETF systems: rep-rated driver, beam propagation, automated target fabrication, target injection, coolant circulation, and chamber exhaust. This goal is listed first because it is a prerequisite for accomplishment of the other goals.

*The group included representatives of LLNL, LANSL, Sandia, OIF-DOE, EPRI, ETEC, TRW, Bechtel, Grumman Aerospace, Westinghouse, the Univ. of Wisconsin, and the Univ. of Rochester.

Energy Applications R&D

o The key design issue is thermal and mechanical response of the first wall protection material (gas, liquid, or solid) to the fusion pulses and the subsequent loading of the structure. Although theoretical analyses will continue to be performed for different chamber concepts, full-scale experimental verification is essential because of the complex synergistic phenomena involved. We expect that some current chamber concepts will be eliminated through analysis and nonnuclear experiments before the ETF is completed. Those concepts that do qualify may have differing test objectives, such as those described below for four different wall concepts:

oo Dry wall. The amount of wall ablation or debris buildup and the transient structural loads must be determined, and the first-wall integrity must be verified. If the wall is also magnetically protected, the interaction of the target debris with the magnetic field must be determined.

oo Gas-protected wall. The gas deposition profiles for x rays and debris, the blast-wave loading of the structure, and the transient heat transfer through the gas must be determined for a variety of target designs, gas compositions, and gas pressures.

oo Wetted wall. The magnitude and duration of the pressure pulse transmitted to the structure from the fusion-heated liquid must be verified, and the subsequent motion of the liquid wall and ablated gas must be tracked.

oo Liquid-metal wall. Jet disassembly characteristics, liquid-liquid interactions, ablated-gas behavior and gas/liquid loads on the structure must all be measured.

o The chamber atmosphere must be restored to acceptable levels of pressure and temperature before the next target is injected and the next driver pulse is propagated. Early in the interpulse time, the chamber atmosphere includes extremely hot material (e.g., debris ions,

Energy Applications R&D

heated chamber gas, and vaporized liquid- or solid-wall material), and the vacuum systems must either be able to cope with these materials or be capable of interrupted operation. The return to nominal first-wall conditions must be verified.

- o Heat removal must be verified. The structure is heated both directly and by thermal contact with its protective material (gas, liquid, or solid). The ETF must verify the scheme used to cool the structure.

- o The pressure pulses produced in blanket liquids by pulsed neutrons will be measured by the ETF, as will the streaming of neutrons down beam lines and vacuum ports. Although facility lifetime precludes full-scale testing, the ETF will be capable of producing observable radiation damage in small samples mounted near the source. Between 10^{18} and 10^{21} n/cm² are required depending on the material and the effect. For example, at a 10-cm distance from a 25-MW source, 10^{18} neutrons/cm² will be accumulated in ~140 s. About 10% of the facility life would be required to produce 10^{21} n/cm² at a distance of 10 cm from a 25-MW source. These experiments, which will contrast pulsed neutron damage with steady neutron damage from facilities such as the Rotating Target Neutron Source (RTNS) or the Fusion Materials Irradiation Test facility (FMIT), will be essential for the design of an ICF materials test facility.

- o The chemistry of contaminants (target debris, ablated wall materials, and corrosion products) in the chamber gas and coolant will be studied with the ETF to verify the capability of remotely processing these fluids. Because of the facility's low duty cycle, this area of interest will be explored between experiments.

- o The safety and remote operation and maintenance of a facility containing radioactive materials and, possibly, large quantities of liquid metal will be a key demonstration goal of the ETF.

Energy Applications R&D

Sizing the ETF

The size of a magnetic-fusion ETF is determined by the required plasma parameters; e.g., the Tokamak ETF will be 600 to 750 MW_t. In ICF, however, the plasma is decoupled from the reactor, and the ETF power is based on duplicating reactor parameters such as first-wall fluence and blanket power density. Because some design issues depend on power, while others depend on fusion-pulse energy, it is appropriate to design the ETF to operate at the full reactor repetition-rate. There is general agreement that a 25-MW_f facility, operating with a 1.0- to 1.5-MJ driver and gains in the range of a few to a few tens at 1 to 10 Hz, is all that is required. These operating conditions are compatible with conservative gain-curve estimates.¹

First wall fluence is the key design parameter for the dry-wall, magnetically protected-wall, and wetted-wall reactor concepts, and the wall radius required to achieve full-scale first-wall fluences in a 25-MW_f ETF is between 0.5 and 1.0 m for these three concepts. For the gas-protected wall, the key parameter could be either first-wall fluence or chamber power density. For the 20-Hz SOLASE gas-protected-wall reactor concept, these reactor-scale parameters are duplicated at radii of 0.6 and 1.2 m, respectively, for a 25-MW_f ETF.

For the HYLIFE liquid-metal-wall reactor concept, the key design parameters are the neutron energy density in the inner portion of the jet array and the soft x ray and debris fluence on the inner surface of the jet array. For a 100-MW_(f) ETF, full-scale reactor midplane conditions are duplicated when the inner radius of the jet array is 0.1 to 0.15 m. Thus, a 25-MW ETF would be about one-quarter scale for HYLIFE.

The engineering impact of a low-power ETF is considerable, and we do not have to utilize or wait for the development of high-gain targets

Energy Applications R&D

(which can proceed in parallel). Low power minimizes the heat transfer and vacuum pumping requirements, as well as the costs. In addition, low power also means that the facility will be easier to operate and maintain and that tritium fueling costs will be reasonable (~ \$20,000/yr at \$8/mg).

Because all of the current reactor candidates require about the same size chamber, and because they all could use the same heat-removal and other supporting systems, sequential testing of multiple reactor concepts in the ETF may be feasible and cost-effective.

Cost of the ETF

The conservative target-gain curves indicate that a 1.0- to 1.5-MJ on-target short-wavelength laser or heavy-ion beam could drive a 25-MW_f ETF at reactor rep-rates. Because of the low thermal power and driver energy, unit costs for individual subsystems such as the driver (\$/MJ), liquid metal pumps (\$/MW), or target factory (\$/target) can be much higher than allowable unit costs in a commercial plant and still result in an ETF cost that is reasonable. A cost scoping study for an ICF-ETF has begun.

Conclusions

We have enlisted the advice of a broad spectrum of fusion-engineering experts to begin the planning for an engineering test facility (ETF) for inertial confinement fusion (ICF). We concentrated on setting the objectives for such a facility, listing the development requirements for each reactor concept, and defining the appropriate size and time scale.

Energy Applications R&D

A small, 25-MW_f, device, operating with modest target gains in the range of 3 to 30 at reactor pulse-rates, appears to be sufficient to attain engineering objectives comparable to those in the MFE Tokamak program, which will require a 600- to 750-MW_f device. Therefore, a single-pulse test facility (SPTF), designed to develop the high gains required for a power plant (≥ 200) or to demonstrate significant military applications, does not have to precede the ETF. SPTF could be operated concurrently with 2 ETF, perhaps using a shared driver. An ETF that does not require high gains or high power levels can provide potentially significant savings in both development time and cost and is, therefore, an important opportunity for ICF.

1. K. A. Brueckner, et. al. Assessment of Drivers and Reactors for Inertial Confinement Fusion, Electric Power Research Institute Report AP-1371 (Feb. 1980).

LLNL Publications

K. Whitham, M. M. Howland, and J. R. Hutzler, High Density Energy Storage Capacitor, Lawrence Livermore National Laboratory, Livermore, Calif., UCRL-82937. (Prepared for 8th Symposium on Engineering Problems of Fusion Research, San Francisco, Calif., Nov. 13-16, 1979.)

B. W. Weinstein and J. T. Weir, Measurement of Tracer Elements in Inertial Fusion Target Fuel, Lawrence Livermore National Laboratory, Livermore, Calif., UCRL-83150 (Rev. 1). (Prepared for J. Appl. Phys., Nov. 9, 1979)

J. E. Andrews, Jr., and J. C. Koo, Surface Treatment of Lead Glass Microsphere, Lawrence Livermore National Laboratory, Livermore, Calif., UCRL 83398. (Prepared for Topical Meeting on Inertial Confinement Fusion, San Diego, Calif., Feb. 26-28, 1980.)

R. D. Boyd, Evolution of Shiva Laser Alignment Systems, Lawrence Livermore National Laboratory, Livermore, Calif. UCRL-84008. (Prepared for SPIE Proceedings from 24th Annual Technical Symposium, San Diego, Calif., July 28 through Aug. 1, 1980.)

J. H. Eberly, M. J. Konopnicki, and B. W. Shore, The Influence of Propagation on Off-Resonant Molecular Excitation, Lawrence Livermore National Laboratory, Livermore, Calif., UCRL-84259 (Rev. 1). (Prepared for International Quantum Electronics Conference, Boston, Mass., Apr. 23, 1980.)

M. J. Weber and R. M. Almeida, Large Stimulated Emission Cross Sections of Nd³⁺ in Chlorophosphate Glass, Lawrence Livermore National Laboratory, Livermore, Calif., UCRL-84595. (Prepared for J. Non-Cryst. Solids, June 24, 1980)

INTERNAL DISTRIBUTION

1A H. G. Ahlstrom
2A L. P. Altbaum/E. G. English
3A J. D. Anderson
4A R. T. Andrews
5A D. T. Attwood
6A R. B. Barker
7A R. E. Batzel/R. L. Wagner
8A C. F. Bender
9A J. I. Davis
10A G. D. Dorough
11A J. L. Emmett
12A T. K. Fowler
13A E. K. Freytag
14A A. J. Glass
15A R. O. Godwin
16A J. R. Greenwood
17A A. C. Hausmann
18A C. D. Hendricks
19A J. F. Holzrichter
20A J. T. Hunt
21A J. D. Immele
22A J. S. Kahn
23A R. E. Kidder
24A W. L. Kruer
25A W. F. Krupke
26A E. A. Lafranchi
27A J. D. Lindl
28A W. H. Lowdermilk
29A K. R. Manes
30A L. L. Marino
31A M. M. May
32A H. C. McDonald/W. F. Arnold
33A G. H. Miller
34A M. J. Monsler
35A R. D. Neifert
36A J. H. Nuckolls/J. C. Stevens
37A R. L. Pond
38A H. L. Reynolds
39A H. P. Sartorio
40A H. D. Shay
41A V. W. Slivinsky
42A W. B. Shuler
43A W. B. Simecka
44A A. Szoke
45A C. B. Tarter
46A A. Toor
47A T. Wainwright
48A M. J. Weber
49A M. M. Wilkins
50A R. D. Woodruff
51A G. B. Zimmerman

EXTERNAL DISTRIBUTION

52A G. Canavan
53A T. F. Godlove
54A C. B. Hilland
55A O. Lewis
56A S. L. Kahalas
57A K. G. Gilbert
58A J. P. Murphy
59A C. E. Rossi
60A R. L. Schriever
61A T. A. Walsh
Office of Laser Fusion
U. S. Department of Energy
Washington, D. C. 20545
62A D. C. Sewell
U. S. Department of Energy
Office of Assistant Secretary
of Defense Programs
Washington, D. C. 20545
63A K. J. Adney
U. S. Deptment of Energy
Office of Classification
Washington, D. C. 20545
64A J. J. Stekert/R. L. Bingham
U. S. Department of Energy
Office of Policy and Evaluation
Washington, D. C. 20585
65A Z. N. Zafiris
U. S. Department of Energy
San Francisco Operations Office
1333 Broadway
Oakland, CA 94612
66A D. B. Henderson
Los Alamos Scientific Laboratory
P. O. Box 1663
Los Alamos, NM 87545
67A S. Rockwood
Director of Inertial Fusion
Los Alamos Scientific Laboratory
Los Alamos, NM 87545
68A R. Selden
X Division Leader
Los Alamos Scientific Laboratory
P. O. Box 1663
Los Alamos, NM 87545

EXTERNAL DISTRIBUTION (cont'd.)

69A D. Wilson
Los Alamos Scientific Laboratory
P. O. Box 1663
Los Alamos, NM 87545

70A G. Yonas
P. O. Box 5800
Albuquerque, NM 87185

71A C. A. McDonald
R & D Associates
P. O. Box 9695
Marina Del Rey, CA 90291

72A J. R. Cooper
R. & D. Associates
1401 Wilson Blvd.
Arlington, VA 22209

73A-74A File